

Sneutrino Mass Measurements at e^+e^- Linear Colliders

J. Kenichi Mizukoshi¹, Howard Baer², A. S. Belyaev² and Xerxes Tata¹

¹*Department of Physics and Astronomy, University of Hawaii, Honolulu, HI 96822, USA*

²*Department of Physics, Florida State University, Tallahassee, FL 32306 USA*

Abstract

It is generally accepted that experiments at an e^+e^- linear collider will be able to extract the masses of the selectron as well as the associated sneutrino with a precision of $\sim 1\%$ by determining the kinematic end points of the energy spectrum of daughter electrons produced in their two body decays to a lighter neutralino or chargino. Recently, it has been suggested that by studying the energy dependence of the cross section near the production threshold, this precision can be improved by an order of magnitude, assuming an integrated luminosity of 100 fb^{-1} . It is further suggested that these threshold scans also allow the masses of even the heavier second and third generation sleptons and sneutrinos to be determined to better than 0.5% . We re-examine the prospects for determining sneutrino masses. We find that the cross sections for the second and third generation sneutrinos are too small for a threshold scan to be useful. An additional complication arises because the cross section for sneutrino pairs to decay into any visible final state(s) necessarily depends on an unknown branching fraction, so that the overall normalization is unknown. This reduces the precision with which the sneutrino mass can be extracted. We propose a different strategy to optimize the extraction of $m(\tilde{\nu}_\mu)$ and $m(\tilde{\nu}_\tau)$ via the energy dependence of the cross section. We find that even with an integrated luminosity of 500 fb^{-1} , these can be determined with a precision no better than several percent at the 90% CL. We also examine the measurement of $m(\tilde{\nu}_e)$ and show that it can be extracted with a precision of about 0.5% (0.2%) with an integrated luminosity of 120 fb^{-1} (500 fb^{-1}).

I. INTRODUCTION

There have been many studies [1,2] that have pointed out the complementarity between experiments at the Large Hadron Collider (LHC) and at e^+e^- linear colliders (LC) that are being considered as the next major high energy accelerator facility after the LHC. High energy hadron colliders with general purpose hermetic detectors are ideal for broad band searches of new phenomena [3,4]. While some recent studies (performed within the context of specific supersymmetric models) have shown that it may be possible to make precision measurements of masses (more specifically, mass differences) [3,5–7] and possibly other attributes of new particles [8], experiments at the LC allow a relatively model-independent determination of masses [9–14] and other properties of Higgs bosons and supersymmetric (SUSY) particles assuming that these are kinematically accessible, in addition to more detailed [15,16] measurements specific to particular models.

The original studies [9,10] of sparticle mass measurements at linear colliders rely largely on kinematic reconstruction of masses; *e.g.* for the measurement of $m(\tilde{e}_R)$, the energy distributions of the electrons in $\tilde{e}_R \rightarrow e\tilde{Z}_1$ is, except for effects of cuts and resolution smearing, flat with sharp end points determined only by $m(\tilde{e}_R)$ and $m(\tilde{Z}_1)$. It has been shown that with several tens of fb^{-1} , experiments at LCs should measure these masses with a precision at the percent level. A similar precision was shown to be possible for the determination of the lighter chargino mass, even though the energy spectrum of the visible daughters is not flat. The same idea was extended to sparticles decaying via cascades; *e.g.* $\tilde{\nu}_e \rightarrow e\tilde{W}_1$, $\tilde{W}_1 \rightarrow f\tilde{f}'\tilde{Z}_1$, ($f = q, \mu$). The end points of the electron energy distribution are determined by just $m(\tilde{\nu}_e)$ and $m(\tilde{W}_1)$. Again, these sparticle masses were shown to be measurable at the 1-2% level [11–13]. In all these studies, longitudinal polarization of the electron beam was essential to control Standard Model (SM) backgrounds and SUSY contamination.

Very recently, in the TESLA Technical Design Report [14], it has been emphasized that the tunability of the energy of a LC may be used to perform an energy scan close to a new production threshold. It is claimed that in some cases ($\tilde{W}_1, \tilde{e}_L, \tilde{e}_R, \tilde{\nu}_e$) this allows sparticle masses to be determined with a precision of a part per mille at a LC. Specifically, it was suggested that this could be achieved by a threshold scan of the cross section (10 points spaced 1 GeV apart with an integrated luminosity of $10 \text{ fb}^{-1}/\text{point}$) in any particular channel chosen so that SM backgrounds and SUSY contamination is small. Further, these results were extrapolated to argue that masses of the heavier sleptons of the second and third generations ($\tilde{\mu}_L, \tilde{\nu}_\mu, \tilde{\tau}_2$ and $\tilde{\nu}_\tau$) could also be measured with a precision of about 0.5%. For the measurements of third generation sleptons, it was assumed that secondary vertex detection would serve to efficiently tag tau leptons. Without making any representation about whether or not this is possible, we will assume this to be true for our analysis. We will, therefore, optimistically assume that light flavour and gluon jets are not a background for hadronically decaying taus, and further, that leptonically decaying isolated taus will always be distinguished from prompt es and μs by their displaced vertices.

If sparticle masses can indeed be determined with the impressive precision listed in Ref. [14] it should serve to strigently test various models of how SUSY breaking is mediated to the superpartners of SM particles. Blair, Porod and Zerwas [17] have clearly illustrated how such measurements could be used to test scalar mass unification expected within the mSUGRA framework. In Ref. [18] it is shown how precise determination of the light chargino

and both selectron masses could be used to determine the intra-generational slepton mass splitting at the grand unification scale. This, in turn, will allow distinction between the mSUGRA and the minimal gaugino mediation [19] framework for which the sparticle mass spectra are qualitatively very similar. Measurements of third generation sparticle masses are particularly interesting since these may contain information about the Yukawa sector which may be otherwise difficult to obtain. For instance, determination of $m(\nu_{\tilde{\tau}})$ with a precision of 2-3% could provide striking confirmation of tau neutrino Yukawa interactions [20].

It is clear from these considerations that if sparticle masses can be determined at the part per mille or even the subpercent level, measurements at a LC would provide extremely stringent tests of the underlying framework. In view of its potential importance, we felt that the precision claimed in Ref. [14] warranted a careful re-examination. In this paper, we examine in detail the prospects of measuring second and third generation sneutrino masses via the energy dependence of the cross section. Within all SUSY models with lepton flavour conservation these are produced only via s -channel Z exchange and the cross sections are rather small, just a few GeV beyond the production threshold. The electron sneutrino case is somewhat different because it typically has a much larger cross section since it can also be produced via chargino exchange in the t -channel. Moreover, selectron and $\tilde{\nu}_e$ pair production (due to the much larger production cross section) can be a significant source of SUSY contamination for the $\tilde{\nu}_\mu$ or $\tilde{\nu}_\tau$ signal. We find that at least for the second and third generation sneutrinos, the event rate in relatively background free channels is too small to allow a threshold scan. Instead we propose an alternative strategy by which the mass may be extracted and make projections for the precision with which this might be possible. While our focus is on electron and muon type sneutrinos, for completeness we also examine the precision with which $m(\tilde{\nu}_e)$ might be obtained at a LC.

We base our results on the analysis of two mSUGRA case studies with somewhat different kinematics and cascade decay patterns of sneutrinos. The first case is the one examined in the TESLA Technical Design Report [14] for which the parameters are,

$$\text{Case I : } m_0 = 100 \text{ GeV}, m_{1/2} = 200 \text{ GeV}, \tan \beta = 3, A_0 = 0, \mu > 0.$$

The second case that we choose was studied in Ref. [20] to gain some idea of how well the tau sneutrino mass could be extracted. The corresponding model parameters are,

$$\text{Case II : } m_0 = 150 \text{ GeV}, m_{1/2} = 170 \text{ GeV}, \tan \beta = 5, A_0 = 0, \mu > 0.$$

Several sparticle masses along with relevant branching fractions are shown in Table I. We see that for both these cases m_h the mass of the lightest neutral scalar in the Higgs boson sector is well below the current LEP bound [21] of 113 GeV so that it is quite likely that these cases are experimentally excluded. The reason that we have chosen these cases is to facilitate comparisons with the earlier studies where the precision with which the sneutrino masses could be obtained was also examined.¹ We should mention a peculiar feature of Case I. Here, $m(\tilde{Z}_2)$ is just slightly larger than $m(\tilde{\tau}_1)$ so that the decay $\tilde{Z}_2 \rightarrow \tilde{\tau}_1 \tau$ competes with other three-body decays. The decay patterns of \tilde{Z}_2 are thus unusually sensitive to the mass spectrum, and indirectly therefore, also to our choice $m_t = 175$ GeV.

¹The value of m_h is quite irrelevant to our analysis.

The remainder of this paper is organized as follows. In the next section, we compare the technique based on the energy dependence of the cross section (of which the threshold scan is a particular case) with that based on kinematic reconstruction of masses as in earlier studies [9–13]. We point out some issues that potentially degrade the mass precision that will be attained in experiments at a LC. In Sec. III we propose how one might optimize an energy scan in relatively clean channels where the signal is rate-limited so that a threshold scan is not possible because the signal is tiny in the vicinity of the threshold. In Sec. IV we apply this method and assess how accurately $m(\tilde{\nu}_\mu)$ and $m(\tilde{\nu}_\tau)$ might be determined in experiments at a LC. We also examine the precision with which the electron sneutrino mass might be measured. In Sec. V, we examine other potential channels for the extraction of $m(\tilde{\nu}_\tau)$ and $m(\tilde{\nu}_\mu)$ but find that these suffer from significant backgrounds; in contrast, for $m(\tilde{\nu}_e)$ we find that some improvement may be possible, at least in favourable cases, by combining the signal on several channels. We present a summary of our results along with general conclusions in Sec. VI.

II. PROBLEMS OF DETERMINING SNEUTRINO MASSES VIA AN ENERGY SCAN

The extraction of the sneutrino mass from the energy dependence of the cross section is essentially a counting experiment. We have either to work in a channel that is relatively free of SM background and contamination from other SUSY sources, or develop a procedure for reliably subtracting these backgrounds. Generally speaking, the latter would be preferable in that it allows for a larger signal (since we do not have to limit ourselves to any particular channel) but we will see later that both SM backgrounds as well as SUSY contamination can be large. Moreover, in many SUSY models, all three generations of sneutrinos are expected to be approximately degenerate; as a result, the background from $\tilde{\nu}_e\tilde{\nu}_e$ production to second or third generation sneutrino production will have essentially the same energy dependence, and so will be difficult to subtract in a reliable manner using the data below the signal threshold. In the following we will, therefore, mainly focus our attention on the $\tilde{\nu}_\tau\tilde{\nu}_\tau \rightarrow \tau\tilde{W}_1\tau\tilde{W}_1 \rightarrow \tau\tau jj\ell + \cancel{E}_T$ ($\mu\mu jj\ell + \cancel{E}_T$) channel with $\ell = e, \mu$ where both SM backgrounds as well as SUSY contamination to $\tilde{\nu}_\tau$ ($\tilde{\nu}_\mu$) pair production are relatively small for a right polarized electron beam.² The inclusion of other channels results in substantial SM background and/or SUSY contamination as discussed in Sec. V.

In Fig. 1, we show contours of sneutrino mass as well as those for the branching fraction for the decay chain, $\tilde{\nu}_\tau\tilde{\nu}_\tau \rightarrow \tau\tilde{W}_1\tau\tilde{W}_1 \rightarrow \tau\tau q\tilde{Z}_1\ell\nu\tilde{Z}_1$ in the $m_0 - m_{1/2}$ plane for $A_0 = 0$ and $\mu > 0$. This is the sign of μ favoured by the E821 experiment [22]. For this sign of μ the chargino tends to be lighter so that there is more phase space for the cascade decay of the

²This is the analogue of the $eejj\mu$ channel used for the extraction of the electron sneutrino mass from the energy distributions of electrons from $\tilde{\nu}_e \rightarrow e\tilde{W}_1$ decay [11]. In this study, where it was important not to confuse a lepton from chargino decay with the electron from the primary decay of the sneutrino, this lepton was required to be μ . Here, since we do not need to identify the lepton from sneutrino decay, we allow this to be either e or μ to increase the signal.

sneutrino. We illustrate the contours for *a*) a low value of $\tan\beta = 3$ and *b*) a high value of $\tan\beta = 40$. Also shown is the contour of $m_{\tilde{W}_1} = 100$ GeV which is roughly its lower mass limit³ from LEP experiments [21]. The selectrons are heavier than 100 GeV throughout both planes. The dark shaded region in frame *b*) is excluded because $m^2(\tilde{\tau}_R) < 0$, while the light shaded region is disfavoured because $m(\tilde{\tau}_1) < m(\tilde{Z}_1)$. The branching ratio falls off to below 1% for large values of $m_{1/2}$ because the decay $\tilde{W}_1 \rightarrow \tilde{\tau}_1\nu_\tau$ becomes dominant. We see that Case II which has a branching fraction of 9.7% for this cascade decay chain is very typical as long as the two body decay of the chargino into the lighter stau is kinematically forbidden. Case I, while not atypical, has the corresponding branching fraction towards the lower end of its range within this framework.

Longitudinal electron beam polarization is very effective in removing both SM background as well as SUSY contamination [9,10]. Polarization of the positron beam would also help (if it is achieved without significant loss of luminosity) because the signal cross section increases, but since the availability of polarized positron beams appears less certain, we perform the bulk of our analysis for unpolarized positron beams. To identify potential sources of SUSY contamination and also to show how these might be reduced, we show in Fig. 2 the production cross sections for the most important SUSY processes as a function of the electron beam polarization parameter $P_L = f_L - f_R$, where f_L (f_R) is the fraction of left handed (right handed) electrons in the beam. These have been obtained using ISAJET v7.51 [23]. The two frames respectively show the cross sections for (*a*) Case I, and (*b*) Case II introduced in the previous section. Except for $\tilde{\mu}_L\tilde{\mu}_R$ production which has a negligible cross section, the cross section for smuon pair production is close to that for the corresponding third generation sparticle production with $\tilde{\tau}_1$ ($\tilde{\tau}_2$) replacing $\tilde{\mu}_R$ ($\tilde{\mu}_L$). The obvious point to note is that for signals of second or third generation sneutrinos, a (dominantly) right handed electron beam reduces SM backgrounds from WW and WWZ [24] production as well as SUSY contamination from the largest visible SUSY processes.⁴ In the rest of our analysis, we fix $P_L(e^-) = -0.9$.

To get some idea of the signal rates near threshold, we show the number of $eejj\ell$ events expected (before any cuts) from $\tilde{\nu}_e\tilde{\nu}_e \rightarrow e\tilde{W}_1e\tilde{W}_1 \rightarrow ejj + e\ell\nu + \cancel{E}_T$ ($\ell = e, \mu$) production (solid) and from $\tilde{\nu}_\mu\tilde{\nu}_\mu \rightarrow \mu\tilde{W}_1\tilde{Z}_2\nu \rightarrow \mu jj + ee + \cancel{E}_T$ production (dashed) for $P_L(e^-) = 0.9$ in Fig. 3*a*. For brevity, we show this only for Case I but the results for Case II are qualitatively similar. The higher sneutrino production cross section in Case I is partly compensated by the fact that the branching ratio for the particular cascade decay chain is correspondingly smaller. Following Ref. [14], we assume an integrated luminosity of 10 fb^{-1} for each value of \sqrt{s} , and take the scan to extend to about 10 GeV above the threshold. As discussed previously, the SUSY contamination exemplified by the dashed curve is tiny (the threshold for $\tilde{\ell}_L\tilde{\ell}_L$ production is beyond the range in the figure), and the signal rates high enough to

³ m_h is below the current LEP bound especially for the $\tan\beta = 3$ case, as we have already mentioned.

⁴Since $\tilde{e}_R \rightarrow e\tilde{Z}_1$, $\tilde{e}_R\tilde{e}_R$ production does not contaminate the signal.

imagine carrying out a measurement of $m(\tilde{\nu}_e)$ via a threshold scan as suggested in Ref. [14].⁵ A potential difficulty with this strategy is discussed shortly.

In Fig. 3b we show the corresponding expectations for the $\tau\tau jj\ell$ channel, the favoured final state from tau sneutrino pair production. The $\tilde{\nu}_\tau$ signal cross section is shown as the dotted curve, while the solid and dashed curves denote contamination from electron and muon sneutrinos, respectively. Notice that we have flipped the electron beam polarization. We see from Fig. 2 that while there is slight reduction of the $\tilde{\nu}_\tau$ signal due to the polarization, the contamination from $\tilde{\nu}_e\tilde{\nu}_e$ production is greatly reduced. For $P_L(e^-) = 0.9$, we have checked that the contamination from $\tilde{\nu}_e$ pairs is an order of magnitude larger than the stau signal!⁶ The most striking feature of the figure is that even before experimental cuts and efficiencies are included, the signal yields just a fraction of an event throughout the range of the scan. The availability of positron polarization increases the cross section; for $P_L(e^+) = 0.6$ (corresponding to a positron beam with a dominantly singlet component), the rate is higher by about 30-40%, but clearly this is still insufficient for our purpose. Furthermore, even in this “clean” channel contamination from other sneutrinos is very significant, and this contamination will be present in all SUSY models where the different flavours of sneutrinos are approximately degenerate.⁷ Finally, we remark that although we have not shown this explicitly, very similar considerations will apply to the $\mu\mu jj\ell$ signal from $\tilde{\nu}_\mu\tilde{\nu}_\mu$ production. We conclude that given the current projections for the luminosity of a LC, the threshold scan does not seem to be a viable way for precision measurement of second and third generation sneutrino masses, primarily because the cross section in the relatively clean channel is too small.

Although our discussion up to now makes it appear that it should be possible to determine $m(\tilde{\nu}_e)$ rather precisely via a threshold scan, there is one potential difficulty that could significantly degrade the precision from naive expectations [14]. This arises because the cross section for any particular final state depends on the sneutrino mass as well as the *a priori* unknown branching fraction for the cascade of decays into the channel being examined. This is not an issue for the lightest visible SUSY particle which always decays directly to the lightest supersymmetric particle (LSP), but is important for heavier sparticles which are the focus of our analysis. We have checked that if we have measurements only near the threshold, the freedom of the overall normalization greatly degrades the precision, because the change in the cross section due to a slightly different mass can be compensated for by a small change in the branching fraction. For instance, for Case I with $m_{\tilde{\nu}} = 158.3$ GeV,

⁵ $\tilde{\nu}_\tau\tilde{\nu}_\tau$ production leads to events with a τ rather than μ and so serves to contaminate the signal only if the τ decays leptonically, so that this background is below the dashed curve in Fig. 3a. Moreover, with efficient vertex detection this may be reduced even further.

⁶This could be eliminated by requiring $\ell = \mu$ but at a cost of a factor 2 in the already tiny signal.

⁷We should remark that in the case of $\tilde{\nu}_e$ or $\tilde{\nu}_\mu$ pair production, the taus dominantly come from decays of \tilde{Z}_2 produced via $\tilde{\nu} \rightarrow \nu\tilde{Z}_2$, so that $m_{\tau\tau} \leq m_{\tilde{Z}_2} - m_{\tilde{Z}_1}$. It may, therefore, be possible to find cuts to select out $\tilde{\nu}_\tau$ events over $\tilde{\nu}_e$ or $\tilde{\nu}_\mu$ events at some cost to the signal. However, since the signal is so tiny, it did not make sense to explore this any further.

even at $\sqrt{s} = 390$ GeV (which is quite far from threshold), the cross section changes by $\sim 5\%$ if the $m_{\tilde{\nu}}$ is taken to be just 1 GeV larger than its reference value. Thus an observed event level could be equally well fitted by the nominal mass and branching fraction into the channel in question, or by a mass that is 1 GeV heavier and a branching ratio that is 4.6% rather than 4.4%. Thus, *without precise knowledge of the branching ratio, a determination of sneutrino masses at the part per mille or even the subpercent level via a threshold scan seems impossible, at least if backgrounds restrict us to particular final states.* This state of affairs can be ameliorated by a measurement of the event rate sufficiently far from threshold. Here, we assume the LC will first operate at $\sqrt{s} = 500$ GeV, and that the sneutrino threshold does not accidentally lie too close to this. A measurement of the event rate in the continuum is much less sensitive to $m(\tilde{\nu})$ but strongly constrains the branching fraction. The optimal strategy, therefore, involves measurements in the continuum together with measurements closer to the threshold.

A related (though possibly less severe) problem with the claims of very precise determination of masses using the counting experiment strategy is that the production cross section depends on other sparticle masses (*e.g.* of charginos in the case of $\tilde{\nu}_e\tilde{\nu}_e$ production or neutralinos in the case of selectron production). Any uncertainty in these will be reflected in the corresponding uncertainty in the extraction of the selectron/sneutrino mass. For second and third generation sneutrinos this is academic as we will see that their masses cannot be extracted with subpercent precision, and further, that the uncertainty due to the unknown branching fraction is far bigger. For the extraction of the mass of \tilde{e}_R though (where there is no branching fraction uncertainty) [25], and potentially also for the much better determined $m(\tilde{\nu}_e)$, this could be a factor.

Before closing, we should mention that the uncertainty from the unknown branching fraction has not been factored into earlier analyses [11–13] of masses of sparticles that cascade decay to the LSP, so that the precision may also have been over-estimated in these studies. We may expect that this is a less important factor in these studies since the end points of the energy distributions are determined by just the kinematics of the decay, and are independent of the precise branching fraction for the decay chain.

III. OPTIMIZING THE STRATEGY FOR COUNTING EXPERIMENTS WITH SMALL SIGNAL RATES

The considerations of the previous section make it clear that for rate limited final states such as $\tilde{\nu}_\mu\tilde{\nu}_\mu \rightarrow \mu\mu jj\ell + \cancel{E}_T$ or $\tilde{\nu}_\tau\tilde{\nu}_\tau \rightarrow \tau\tau jj\ell + \cancel{E}_T$ the strategy suggested in Ref. [14], *viz.* measuring the cross section at ten points spaced 1 GeV apart starting just above the threshold, is not feasible. First, the smallness of the cross section necessitates that the available integrated luminosity be distributed over fewer points, and second, we must have a measurement of the cross section far above threshold. The goal of this section is to study how a given integrated luminosity (which we take to be 120 fb^{-1}) ought to be distributed to optimize the extraction of the sneutrino mass. Since our purpose here is only to develop a suitable strategy, for now, we assume the ideal case of 100% detection efficiency and geometric coverage for the detector and ignore backgrounds from SM or other SUSY sources. Our considerations will thus apply equally well to $\tilde{\nu}_\tau$ and $\tilde{\nu}_\mu$ since the production rates and decay patterns are virtually identical for the small value of $\tan\beta$ used in the

analysis. In Sec. IV, where we apply this strategy, the effects of cuts, detection efficiencies and backgrounds will be included.

The energy and sneutrino mass dependence of the cross section for $e^+e^- \rightarrow \tilde{\nu}_\tau \tilde{\nu}_\tau \rightarrow \tau\tau jj\ell + \cancel{E}_T$ can be written as,

$$\sigma(e^+e^- \rightarrow \tilde{\nu}_\tau \tilde{\nu}_\tau) = A \frac{s}{(s - M_Z^2)^2 + M_Z^2 \Gamma_Z^2} \left(1 - \frac{4m_{\tilde{\nu}_\tau}^2}{s}\right)^{3/2}, \quad (1)$$

where the normalization A includes the products of branching fraction for decays to the $\tau\tau jj\ell$ final state. We assume that the available integrated luminosity \mathcal{L} is divided up as $\mathcal{L} = \mathcal{L}_0 + \mathcal{L}_{low} = 120 \text{ fb}^{-1}$, where \mathcal{L}_0 is the integrated luminosity at the nominal machine energy $\sqrt{s_0}$ which we take to be 500 GeV, and \mathcal{L}_{low} the integrated luminosity divided up between N lower energy points between the threshold and $\sqrt{s_0}$. We assume that these points are equally spaced starting at an energy D above the production threshold, and parametrize their locations by,

$$\sqrt{s_i} = 2m_{\tilde{\nu}_\tau} + D + (i - 1)\Delta, \quad i = 1, \dots, N. \quad (2)$$

Our problem then is to choose \mathcal{L}_0, D, Δ and N so as to optimize the mass determination.

Choosing D as small as possible seems to be intuitively optimal as long as the event rate is sufficiently large. In our analysis, we require that there be at least 10 events at each point.⁸ This severely restricts D , because going too close to the threshold results in a smaller number of events. We then distribute the luminosity \mathcal{L}_{low} over the N points so that we expect about the *same number of events at each of these points*. This ensures that the cross sections at each energy are measured with similar precision, but requires that more of the luminosity is spent close to threshold relative to higher energies.

We then proceed as follows. For a particular choice of \mathcal{L}_0, D, Δ and N , we generate a set of Monte Carlo data for model parameters corresponding to Case I so that for each value of $\sqrt{s_i}$ the number of events in the “data” is a Gaussian fluctuation about its theoretical expectation. Next, we fit this “data” to the theory (1), varying the sneutrino mass and the branching ratio BR (implicitly contained in the parameter A) into the $\tau\tau jj\ell$ final state, and obtain the best fits to these two quantities by minimizing χ^2 . The best fit values of $m_{\tilde{\nu}}$ and BR do not, of course, coincide with their “input values”. Finally, we compute $\Delta\chi^2 = \chi^2 - \chi_{min}^2$ for different theories with slightly different values of $m_{\tilde{\nu}}$ and BR , and obtain the contour with $\Delta\chi^2=4.61$ which yields the 90% CL limits on how well these parameters might be determined experimentally for the chosen values of \mathcal{L}_0, Δ and N . The procedure is then repeated to optimize this choice.

We found that choosing N to be too large was far from optimal because the event rate is small. The choice $N = 10$ as in Ref. [14] resulted in a very poor determination of the mass parameter. The best results were obtained for $N \leq 3$. An illustrative example of our results is shown in Fig. 4 for $N = 3, \Delta = 5 \text{ GeV}$ and $a) \mathcal{L}_0 = 60 \text{ fb}^{-1}$ (correspondingly, $D = 45 \text{ GeV}$),

⁸Requiring just 10 events before efficiency and acceptance corrections is somewhat over-optimistic, since we will see later that once experimental acceptances and cuts are folded in, the detection efficiency is 10-20% (25-30%) for $\tau\tau jj\ell$ ($\mu\mu jj\ell$) events.

b) $\mathcal{L}_0=40 \text{ fb}^{-1}$ ($D = 32 \text{ GeV}$), c) $\mathcal{L}_0= 20 \text{ fb}^{-1}$ ($D = 26 \text{ GeV}$) and d) $\mathcal{L}_0 = 0$ ($D = 21 \text{ GeV}$). The total integrated luminosity has been taken to be 120 fb^{-1} . We see that for the particular choice of N and Δ , frames b) and c) show the best determination of the sneutrino mass. In frame a) where $\mathcal{L}_0= 60 \text{ fb}^{-1}$ the 10 event requirement does not allow us to sample closer than 45 GeV from the threshold, resulting in a degraded mass measurement. The results in frame d) confirm our earlier discussion: without a measurement in the continuum to constrain the branching fraction, the mass cannot be well determined.

In Fig. 4, we had arbitrarily fixed $\Delta = 5 \text{ GeV}$, a rather small value to simulate an energy scan “close” to threshold. The results of an analysis with variable Δ is shown in Fig. 5. Here, we have fixed $N = 3$, $\mathcal{L}_0 = 20 \text{ fb}^{-1}$ and taken a) $\Delta = 20 \text{ GeV}$ with $D = 19 \text{ GeV}$, b) $\Delta = 40$ with $D = 16 \text{ GeV}$, c) $\Delta = 60 \text{ GeV}$ with $D = 16 \text{ GeV}$, and d) $\Delta = 80$ with $D = 15 \text{ GeV}$. We see that the precision on the mass is considerably improved relative to Fig. 4. This is mostly because for the larger values of Δ in Fig. 5, we can go closer to the threshold because the cross sections at all but the lowest energy point are considerably bigger, so that less luminosity is needed to achieve the 10 event level at these intermediate points. Moreover, we see that frames c) and d) show a comparable precision on the sneutrino mass so that the precise value of Δ is unimportant as long as it is sufficiently large. An important conclusion is that *in a rate limited channel, even allowing a measurement in the continuum, an energy scan close to the threshold does not seem to be the optimal strategy for determining the sneutrino mass.*

We have examined several choices of \mathcal{L}_0 , D , Δ and N to optimize the strategy for extracting the sneutrino mass. We summarize our findings here. For a good mass measurement:

1. It is necessary to go as close to the threshold as possible consistent with the minimum event level. This requires more integrated luminosity at the lower energy point where the cross section is the smallest.
2. It is necessary to have a reasonable cross section measurement well above threshold to constrain the branching fraction. This comes “for free” because presumably the collider will first run at the nominal energy which we have taken to be 500 GeV. We found that out of a total integrated luminosity of 120 fb^{-1} , having about 20 fb^{-1} at $\sqrt{s} = 500 \text{ GeV}$ was optimal.
3. In addition to the lowest energy point and the continuum point, just one or two additional points are needed to get the mass. Having too many points requires the total luminosity to be divided too much resulting in a loss of precision.
4. The precise interval between the points scanned is not very important. It is important, however, that the interval be large enough so that these points are not all concentrated very close to threshold where the cross section is small, and one does not obtain any measurement sufficiently close to the threshold.

In our study, the results in Fig. 5c and d yield about the best measurement of the sneutrino mass. We thus conclude that with an ideal detector and no background, as well as no initial state radiation, beam energy spread or beam-beam interaction effects, the tau sneutrino mass can be determined at about the $\sim 3\%$ level with an integrated luminosity of

120 fb⁻¹, unless the branching fraction for the decay cascade can independently be determined from other measurements.⁹ Even under these idealized circumstances, our conclusions about the precision on the mass that can be attained are considerably more pessimistic than those in Ref. [14]. We see, however, that the energy scan also fixes the branching fraction for the decay to the particular final state to be between 3-6%. It is worth remarking that the branching fraction is slightly better constrained if \mathcal{L}_0 is chosen to be larger, as for example, in Fig. 4a. Before closing this discussion, we should mention that we have ignored effects of the sneutrino widths in our analysis. Since $\Gamma_{\tilde{\nu}}$ is typically a fraction of a GeV, while the smallest value of D is larger than 15 GeV, non-zero width effects [26] are completely negligible.

IV. REALISTIC DETERMINATION OF SNEUTRINO MASSES

In this section we use the energy scan strategy devised in Sec. III to investigate the precision with which the tau and muon sneutrino masses might be measured in LC experiments once effects of finite detector acceptances, experimental cuts, SM backgrounds, SUSY contamination, and finally, beam energy smearing due to initial state radiation (ISR) and beamstrahlung are incorporated.

A. Beamstrahlung and Initial State Radiation

The main effect of beamstrahlung and ISR is to reduce the energy in the electron/positron beams due to emission of photons, thereby reducing the available centre of mass energy in the e^+e^- collision. Since our strategy entails a measurement of the event rate as close to threshold as possible, and the cross section varies rapidly with energy near the threshold, these effects are especially important. We include these effects following the suggestions in Ref. [27]. For ISR, we use the structure function approximation suggested by Skrzypek and Jadach [28]. We include beamstrahlung by using the electron energy spectrum as given by Peskin [27]. We set the parameter $N = N_\gamma/2$ with $N_\gamma = 1.176$ and take $\Upsilon = 0.124$. This choice corresponds to the design parameters in Ref. [29] for $\sqrt{s} = 500$ GeV.

The reduction of $\sigma(\tilde{\nu}_\tau\tilde{\nu}_\tau)$ (or $\sigma(\tilde{\nu}_\mu\tilde{\nu}_\mu)$) is illustrated in Fig. 6. The reduction, which is shown relative to the nominal cross section σ_0 , is a function of just $\sqrt{s}/2m$, where m is the sneutrino mass. The diamonds and triangles show the result for Case I and Case II, respectively, while the line is a fit through the points. We see the striking reduction of the cross section close to the threshold as expected. We will fold this reduction into our evaluation of the energy dependence of the cross section, and into our assessment of the precision with which the sneutrino mass might be measured. We should mention that this is perhaps too conservative since we will use the beamstrahlung parametrization appropriate

⁹One might think that reducing N to 1 would allow a better measurement since D could be chosen to be smaller still. While this may be true, this is not really possible in practice since one would have to know the position of the threshold quite precisely to reduce D significantly.

to a 500 GeV collider all the way down to about 350 GeV where the beamstrahlung and ISR effects, and hence the reduction of the cross section, are smaller.

B. Monte Carlo Simulation

We use ISAJET v7.51 for our SUSY event simulation as well as simulation of $2 \rightarrow 2$ SM backgrounds. We use a toy calorimeter covering $-4 < \eta < 4$ with cell size $\Delta\eta \times \Delta\phi = 0.05 \times 0.05$. Energy resolution for electrons, hadrons and muons is taken to be $\Delta E = \sqrt{.0225E + (.01E)^2}$, $\Delta E = \sqrt{.16E + (.03E)^2}$ and $\Delta p_T = 5 \times 10^{-4} p_T^2$, respectively. Jets are found using fixed cones of size $R = \sqrt{\Delta\eta^2 + \Delta\phi^2} = 0.6$ using the ISAJET routine GETJET (modified for clustering on energy rather than transverse energy). Clusters with $E > 10$ GeV and $|\eta(\text{jet})| < 2.5$ are labeled as jets. Muons and electrons are classified as isolated if they have $E_T > 5$ GeV, $|\eta(\ell)| < 2.5$, and the visible activity within a cone of $R = 0.5$ about the lepton direction is less than $\max(\frac{E_{T\ell}}{10}, 1 \text{ GeV})$. Identification of taus is discussed below. In addition to these basic acceptance cuts, we also require $\cancel{E}_T \geq 25$ GeV to enhance the SUSY signal.

C. Tau Sneutrinos

We focus here on the $\tau\tau jj\ell$ signal that we have been discussing. Here ℓ is defined to be an electron or muon not tagged as coming from tau decay. The cross section in this channel is sensitive to how well taus can be identified. Usually it is assumed that only hadronically decaying isolated taus can be identified as narrow jets with one or three charged tracks¹⁰ with total charge ± 1 and $m_{tracks} \leq m_\tau$, with little hadronic activity around them. This is implemented via a cone algorithm [20] that required the tracks to be in a 10° cone about the jet axis, with no additional hadronic activity in the corresponding 30° cone. For identification of both taus in the $\tau\tau jj\ell$ channel, we then immediately lose a factor 4/9 relative to the corresponding signal for muon sneutrinos. Since the signal in this channel is already small, it is worthwhile to seriously consider any possibility for more efficient τ identification. Following our discussion in Sec. I, we will optimistically assume that *all* leptonically decaying taus (where the secondary leptons satisfy p_T and geometric cuts of the previous subsection) are tagged. ‘‘Tau jets’’ would also have a displaced vertex, but this is also true of heavy flavour jets. Moreover charm has a lifetime and mass similar to tau, so that charm quarks from the decays $\tilde{W}_i \rightarrow cs\tilde{Z}_1$ and $\tilde{Z}_j \rightarrow c\bar{c}\tilde{Z}_1$ would contaminate the tau sample. A c -quark would fragment into a $D^{(*)}$ meson which would rapidly decay to a (weakly decaying) D meson and additional pions or kaons; this lightest of the D mesons would decay weakly, resulting in a displaced vertex due to its long lifetime. If the fragmentation products and the pions/kaons from the strongly decaying $D^{(*)}$ meson are soft, or away from the final weakly decaying D (which has a mass close to m_τ), the c jet can mimic a hadronically decaying τ lepton. Even if it is possible to efficiently discriminate between τ s and b s via the difference

¹⁰A track is required to have a p_T of at least 0.5 GeV.

in their masses and lifetimes, we need to examine whether additional discrimination between tau and charm jets is needed.

Toward this end we have computed the cross section for $4j + \ell$ final state from all SUSY sources, where one of the four jets comes from a hadronically decaying τ and at least one of the remaining three is a charm jet. We find that this cross section is of the same size as the $\tau\tau jj\ell$ signal cross section from hadronically decaying taus, so that with vertexing alone, c jets would significantly contaminate the τ sample making precision measurements impossible. Fortunately, unlike τ jets, most c -jets are not expected to have just three tracks in the 10° cone with no tracks in the larger 30° cone.

To minimize unnecessary loss of the already small $\tau\tau jj\ell$ signal, rather than use the stringent cone algorithm of Ref. [20] for the identification of hadronically decaying τ s and veto jets with a track in the outer cone, we have examined the ratio,

$$r \equiv \frac{\sum_{i=1}^{N^{in}} E_i^{in}}{\sum_{i=1}^{N^{in}} E_i^{in} + \sum_{j=1}^{N^{out}} E_j^{out}}, \quad (3)$$

where N^{in} , which is required to be 1 or 3 and N^{out} are the number of tracks in the 10° and the 10° - 30° cones, respectively. The cone algorithm used earlier requires $N^{out} = 0$; *i.e.* $r = 1$. The dashed (solid) histogram in Fig. 7a shows distribution of r for real τ -jets from $\tilde{\nu}_\tau\tilde{\nu}_\tau$ events for Case I (Case II). The last bin (beyond $r = 1$) shows the event rate for $r = 1$ and contains about 85% of the events. Since we require two taus in our signal, requiring $r = 1$ reduces the cross section from hadronically decaying taus by about 30%. The corresponding distribution from QCD jets in the $\tilde{\nu}_\tau\tilde{\nu}_\tau$ sample which coincidentally have $N^{in} = 1$ or 3 is shown in Fig. 7b. As expected, the distribution is broad because typically QCD jets would have many more tracks than 3 and some of these would lie in the outer cone. The peak at $r = 1$ is presumably either because the jet has only one or three tracks or, by chance, the other tracks happen to be outside the 30° cone.

Assuming the distribution of tracks in c jets is qualitatively similar to that in Fig. 7b, it is clear that requiring $r \geq r_{min} = 0.5 - 0.8$ will reduce the charm contamination with little effect on the signal. We have checked that even with $r \geq 0.5$, the contamination from charm jets in SUSY events is reduced to about 20% of the $\tau\tau jj\ell$ signal from just the hadronically decaying taus. We stress, however, that we view the results of the τ - c discrimination analysis as qualitative. A serious analysis of this should include the r distribution from just c -jets, effects of differences in τ and D meson lifetimes as well as incorporating the (presumably small) contamination from b and light quark jets. Moreover, the results may also be sensitive to the details of the quark fragmentation as well as hadronization. The important message from our discussion, however, is that vertex detection by itself *is not sufficient* to eliminate contamination of τ signals, but with additional requirements this can probably be effectively reduced. We will, therefore, not consider it in the remainder of our analysis.

The importance of being able to tag τ s via their leptonic decays is illustrated in Table II. We show the results for three values of the c - τ discrimination parameter r_{min} . Here j^τ (ℓ^τ) refer to a tau identified via its hadronic (leptonic) decay. The table shows the gain in the case of the hadronically decaying τ s from relaxing the original cone algorithm and including τ -jets with $r < 1$. The result differs somewhat from simple expectations based on Fig. 7 because while *all* taus were included in the figure, here we only include events with two identified taus, two jets and a lepton; *i.e.* the environment of the taus is somewhat

different. The main point of Table II is that if vertex detection allows for efficient tagging of leptonically decaying taus, the signal essentially doubles (and increases by a factor of 3 relative to that using the original cone algorithm). In the following we will use the relaxed cone algorithm with $r_{min} = 0.5$, and assume that leptonically decaying taus can be efficiently tagged.

We are now ready to discuss the prospects for the determination of $m(\tilde{\nu}_\tau)$. Our procedure for this is essentially the same as in Sec. III except that we now include the effects of ISR and beamstrahlung, finite detector acceptances and cuts, and backgrounds. To avoid repeated, lengthy simulations of the signal for each point in the sneutrino mass vs branching fraction plane, we have adopted the following procedure.

1. First, we obtain the total cross section into the $\tau\tau jj\ell$ final state. This step does not entail any event simulation.
2. Second, we correct this cross section for beamstrahlung and ISR effects using the curve in Fig. 6.
3. Third, we multiply the corrected cross section by an efficiency function to take into account the effects of detector acceptance, measurement resolution and experimental cuts. To obtain this we use ISAJET to simulate $\tilde{\nu}_\tau\tilde{\nu}_\tau$ events for SUSY parameters corresponding to the two cases that we have studied. We assume that the efficiency changes slowly over the range of sneutrino masses in our scan, and take it to be a constant.

This procedure allows us to scan the signal in the $m_{\tilde{\nu}} - BR$ plane with just one signal simulation for each of the two cases. Of course, the SUSY contamination has also to be simulated in each case as discussed below.

The detection efficiency for the $\tau\tau jj\ell$ signal is shown in Fig. 8. The diamonds (triangles) show the results of our simulation for Case I (Case II) while the curves, which we will use for our subsequent analysis are a fit. The efficiency varies between about 10-20%. One might think that the main reason for this low efficiency is due to inefficient tau detection, but this is not entirely the case. Requiring five objects inside the detector acceptance together with $E_T \geq 25$ GeV already reduces the efficiency to 25-30% (see Fig. 11 below). The additional reduction is indeed due to differences in tau and muon detectability. The efficiency is significantly smaller in Case I, presumably because the mass difference $m(\tilde{\nu}_\tau) - m(\tilde{W}_1)$ is considerably smaller, resulting in somewhat softer taus than in Case II. The turnover for larger values of \sqrt{s} in Case I is probably due to the fact that sneutrinos are boosted so that their decay products tend to emerge closer in space, and so find it harder to pass the isolation requirements.

In Fig. 9 we show the $\tau\tau jj\ell$ signal along with contamination from various SUSY sources for a) Case I, and b) Case II after all the cuts as well as beamstrahlung and ISR corrections. SM backgrounds from $2 \rightarrow 2$ processes are negligible. $e^+e^- \rightarrow WWZ$ production, where $Z \rightarrow \tau\tau$ and the W s each decay to jj and $\ell\nu$ is a potentially important background. For an electron beam with $P_L(e^-) = -0.9$, the production cross section at $\sqrt{s} = 500$ GeV is just 4.8 fb (in contrast to 40 fb for an unpolarized beam). Folding this with the branching fraction 8.9×10^{-3} for this decay chain yields a background level of just 0.04 fb before any acceptance and identification cuts. Recalling the low detection efficiency for the final state, we conclude

that this background is also negligible. The signal cross section, shown by the solid line, is indeed very small, primarily because of the low detection efficiency. We have separately shown the contamination from the first two generations of sneutrinos and sleptons (circles), $\tilde{\tau}_1\tilde{\tau}_2$ and $\tilde{\tau}_2\tilde{\tau}_2$ production (triangles) and chargino and neutralino production (squares). In the last case, at least one of the charginos or neutralinos is \tilde{W}_2 or $\tilde{Z}_{3,4}$. The reason for separating out the contamination in this manner is that these relative contributions will be model and parameter dependent. In most models (unless $\tan\beta$ is very large) we expect that \tilde{e}_L , $\tilde{\mu}_L$, $\tilde{\tau}_2$ and all three flavours of sneutrinos are approximately degenerate (right handed sleptons and $\tilde{\tau}_1$ pair production does not contribute to the background) and have about the same threshold as the signal. The masses of the heavier charginos and neutralinos are not as directly correlated to $m(\tilde{\nu}_\tau)$ so that the background shown by squares will depend on the model as well as on the choice of parameters. Indeed we see this in the figure. In Case I, this background becomes important only at the highest energy, while in Case II, this is the main background. It may even be that the production of heavy charginos and neutralinos is kinematically inaccessible in a particular model. The dashed line shows the total SUSY contamination. We see that even in this “best channel” the signal to background ratio is $\mathcal{O}(1)$.

The low signal cross section in Fig. 9 means that it is not possible to obtain a mass measurement with just 100 fb^{-1} of integrated luminosity. Even at $\sqrt{s} = 500 \text{ GeV}$, just 2-5 signal events would be expected for an integrated luminosity of 20 fb^{-1} for these cases. We find that for a reasonable mass measurement an integrated luminosity of at least 500 fb^{-1} is necessary. For the remainder of this discussion, we will assume that a data sample of this size will be available. This may be possible with as little as two years [14] to a few years of LC operation at the design luminosity.

We divide this integrated luminosity into \mathcal{L}_0 , which we take to be 100 fb^{-1} , and \mathcal{L}_{low} which, as discussed in Sec. III, we further divide amongst $N = 3$ points to optimize the measurement. Our final result, the 90% CL contour in the $m(\tilde{\nu}_\tau)$ branching ratio plane is shown in Fig. 10 for *a*) Case I, and *b*) Case II. We have required that there be at least six events (after all cuts and beamstrahlung/ISR corrections) at each point. The solid line shows the 90% CL contour assuming that there is no SUSY contamination, while the outer dashed contour is obtained including the background in Fig. 9. The cross shows the result for the best fit for the solid contour; *i.e.* without the background included. Several comments are in order.

- The “error ellipses” from the counting experiment are asymmetric in mass¹¹ in that the lower bound on the mass is further away from the best fit value than the upper bound. In frame *a*) this asymmetry is extreme. While it may be somewhat surprising at first, the asymmetric error ellipse is readily understandable. The point is that if we try to fit the “data” with too high a sneutrino mass, a bad fit is obtained because some of the data points are quite close to the threshold for this fitted mass, resulting in a large χ^2 and a bad fit. On the other hand, if we attempt to fit with too small a

¹¹Indeed the fact that the $\Delta\chi^2 = 4.6$ contours are not ellipses should warn us to view the confidence interval from this as a qualitative indicator since we are clearly in the non-Gaussian regime.

sneutrino mass, the data are much more in the “continuum region” for this value of the sneutrino mass, and there is no data point near the threshold for this mass, so that the fit is not as poor, resulting in an asymmetric ellipse. This argument suggests that no matter how much the integrated luminosity is, there will be a (usually disjoint) region with a small $m(\tilde{\nu})$ and a small branching ratio to compensate the cross section, where the counting experiment alone gives a “good fit” to the data. This would not be a problem if the sneutrino mass in this region is smaller than $m_{\tilde{W}_1}$ which will be measured [9–13] to 1-2% precision by other techniques: sneutrinos with a mass below $m(\tilde{W}_1)$ clearly cannot give the signal we are considering. Our examination of Case I is an extreme case of this phenomenon. The small signal cross section has caused the lower region to merge with the original “ellipse”, but it is not meaningful to think that the sneutrino mass can be smaller than $m(\tilde{W}_1) = 129$ GeV.

- We see that the inclusion of the background indeed reduces the precision with which the mass and the branching ratio can be determined. For the reason just discussed, the background increases the error in the mass more toward the lower end than the upper.
- We should keep in mind that we have examined just two cases. While the SM background is negligible, the SUSY contamination will be model dependent as noted above. Moreover, once the data sample is in hand, a detailed examination of the events may make it possible to reduce the contamination from charginos and neutralinos and possibly also from the first two generations of sneutrinos and sleptons since in these cases the taus are produced from chargino and neutralino decays, while in the signal they result from the primary decay of the produced sparticle. It seems fair, therefore, to say that the precision that might be attained is somewhere between the dashed and solid contours.
- In obtaining the error ellipses, we have taken the SUSY contamination to depend only on the energy; *i.e.* we compute this for the input parameters of the model, and assume that it does not change as we scan the $m_{\tilde{\nu}} - BR$ plane. This is, of course, not true in a particular framework such as mSUGRA or gauge-mediated SUSY breaking where all sparticle masses and couplings are determined by just a few parameters. In these cases, the data would be used to determine these underlying parameters which would then be used to fix for instance $m(\tilde{\nu}_\tau)$. Indeed in particular frameworks, it is entirely possible that the tau sneutrino mass may be much better measured than shown in Fig. 10, since data from $\tilde{\nu}_e\tilde{\nu}_e$ production, which has a two order of magnitude larger cross section, can be used to constrain even $m(\tilde{\nu}_\tau)$. Another way of saying this is that we treat the SUSY contamination as though we are in the MSSM, and (for the purpose of analyzing measurements of $m(\tilde{\nu}_\tau)$) we keep all other sparticle masses fixed. Again we stress that while our analysis suggests that $m(\tilde{\nu}_\tau)$ may only be determined to lie within a ± 8 GeV (± 11 GeV) range without (with) backgrounds in Case II *a model-dependent analysis within a particular framework may yield a much better result.*
- We have checked that our results are quite insensitive to the value of N , as long as it is small. Increasing N to five did not degrade the result much because the best results were obtained for a value of D which was essentially the same as for $N = 3$.

The additional points were at relatively high energy where the integrated luminosity for six events was not very large.

- The dotted contour shows how the solid contour in Fig. 10 would shrink if we increase both \mathcal{L}_0 and \mathcal{L}_{low} by 50%. This roughly corresponds to an increase in the cross section that would be obtained with a positron beam polarization¹² of just over 60%. In frame *a*) we see the emergence of the additional dotted region below $m(\tilde{\nu}_\tau) = 90$ GeV, in accord with our earlier discussion.

We conclude that the energy dependence of the cross section at best allows a measurement of $m(\tilde{\nu}_\tau)$ with a precision of a few percent at the 90% CL. The branching fraction for the decay chain is also constrained.

D. Muon Sneutrinos

The analysis for muon sneutrinos proceeds exactly along the same lines as that for $\tilde{\nu}_\tau$ just discussed. The efficiency¹³ for detecting $\mu\mu jj\ell$ events from the chain $\tilde{\nu}_\mu\tilde{\nu}_\mu \rightarrow \mu\tilde{W}_1\mu\tilde{W}_1 \rightarrow \mu\mu jj\ell + \cancel{E}_T$ is shown in Fig. 11 for the two cases we have been discussing. Again diamonds show the results for Case I while triangles show that for Case II. We see that this efficiency, which typically increases with energy, is about 25-35% for these scenarios.

Fig. 12*a* and Fig. 12*b* show the signal from $\tilde{\nu}_\mu\tilde{\nu}_\mu$ production (solid) along with the SUSY contamination from all charged sleptons and other sneutrinos (circles), and from chargino and neutralino production (squares) for Case I and Case II, respectively. We do not separately show the background from smuons since this has essentially the same threshold as selectrons in most models. The total SUSY contamination is shown as the dashed curve. Except for the fact that the cross sections are higher than in Fig. 9 by a factor 2-3, the two figures are qualitatively very similar. The SM background is again negligible.

The larger efficiency for muon sneutrino events should allow a better determination of $m(\tilde{\nu}_\mu)$. This is borne out by the error ellipses shown in Fig. 13 for *a*) Case I, and *b*) Case II. The solid (dashed) curve shows the result without (with) SUSY contamination. We see that in this case, the impact of the background is much smaller than in our study of $\tilde{\nu}_\tau$. This is presumably because the larger cross section results in a higher statistical significance of the signal. As in Fig. 10, the mass error is asymmetric, but the ellipse is much less skewed primarily because of the higher event rate. Our study shows that assuming that the branching fraction for the decay chain is not constrained from elsewhere, $m(\tilde{\nu}_\mu)$ can be determined to lie between about 148 GeV and 160 GeV (171 GeV and 180 GeV) for

¹²The SUSY contamination also depends on the positron beam polarization and would have to be computed in order to see how the dashed contour is altered.

¹³There is an ambiguity in how we define this efficiency because the decay chain $\tilde{\nu}_\mu\tilde{\nu}_\mu \rightarrow \mu\tilde{W}_1 + \nu\tilde{Z}_2 \rightarrow \mu jj + \mu\mu + \cancel{E}_T$ also leads to the $\mu\mu jj\ell$ final state with $\ell = \mu$. Here, we have defined the efficiency to be what would be obtained assuming the branching ratio is that given just by the decay chain where both sneutrinos decay via their chargino mode.

Case I (Case II), suggesting that counting experiments may determine it with a precision of about $\pm(2.5 - 4)\%$ in a model-independent manner. The branching fraction for the cascade sequence is determined within about $\pm 50\%$ though, once again, with an asymmetric error. This extracted “branching ratio” should, however, be interpreted with care since other decay chains, *e.g.* $\tilde{\nu}_\mu \tilde{\nu}_\mu \rightarrow \mu \tilde{W}_1 + \nu \tilde{Z}_2 \rightarrow \mu jj + \mu\mu + \cancel{E}_T$ also leads to the $\mu\mu jj\ell$ final state (with $\ell = \mu$).

E. Electron Sneutrinos

Although an analysis of how well the electron sneutrino mass can be determined is not the main purpose of this paper, it is a natural extension of the present work. We should state at outset that our study of this is mainly to give the reader an idea of how much the issues raised above, which were very important for the second and third generation sneutrinos, impact on the determination of $m(\tilde{\nu}_e)$. In this case, we do not mean to imply that our study is optimized: indeed in the next section, we will suggest some ways by which the precision may be improved.

For a study of the electron sneutrino, it is clear from Fig. 2 that the electron beam should be polarized to be mostly left-handed. In this case, it is clear that well above the production threshold, the cross section is so large that SM backgrounds as well as SUSY contamination are negligible. What is, however, not clear is whether this will continue to be true close to the electron sneutrino production threshold where the signal becomes small. Since neither SM backgrounds nor the production of lighter charginos or neutralinos is kinematically suppressed at $\sqrt{s} \sim 2m(\tilde{\nu}_e)$, at least some of the channels are likely to be contaminated from these sources. In keeping with the analyses for second and third generation sneutrino masses we will, therefore, first focus on the $eejj\ell$ channel which does not suffer from these backgrounds [11], and defer the question of inclusion of other channels to the next section.

There are two questions concerning the strategy for determining $m(\tilde{\nu}_e)$ that we attempt to answer here. Except for the point at $\sqrt{s} = 500$ GeV that is essential to constrain the branching ratio, is it better to scan several points near the threshold, or is it better that these points be significantly spaced (large Δ) so that we do not spend most of the luminosity where the signal is small? Second, is it better to divide the luminosity equally between the low energy points, or is it best to apportion the luminosity so that we have about an equal number of events for each energy point?

To answer these, we have analysed four distinct strategies for the determination of $m(\tilde{\nu}_e)$. As before, we have first obtained $\sigma(\tilde{\nu}_e \tilde{\nu}_e)$ corrected for beamstrahlung and ISR as before, and then multiplied it by an efficiency function which differs somewhat from that for smuon neutrinos because of the t -channel contribution for $\tilde{\nu}_e \tilde{\nu}_e$ production. We assume there are no SM or SUSY backgrounds to the signal, and require at least six signal events at any energy point.¹⁴

¹⁴For $\tilde{\nu}_\mu$ and $\tilde{\nu}_\tau$ signals, this restricted how close we could go to the threshold. In this case, this is not so for 500 fb^{-1} of integrated luminosity. However, to be able to be very close to the threshold, we already need to have a good idea about $m(\tilde{\nu}_e)$. In our analysis we have conservatively assumed

Our results for the 90% CL ($\Delta\chi^2 = 4.6$) error ellipses in the $m(\tilde{\nu}_e) - BR$ plane are shown in Fig. 14 for Case I (first column) and Case II (second column) for an integrated luminosity of 120 fb^{-1} (outer ellipses) and 500 fb^{-1} (inner ellipses). We divide the luminosity \mathcal{L}_{low} between $N = 3$ points and examine the precision for both $\Delta = 1 \text{ GeV}$ (solid ellipse), and $\Delta = 30 \text{ GeV}$ (dotted ellipse). As in the previous studies, we take \mathcal{L}_{low} to be 100 fb^{-1} (400 fb^{-1}). We perform this analysis first by dividing \mathcal{L}_{low} so that there are an equal number of events for each of the three points (first row), and also equally amongst the three low energy points. Thus, the solid ellipses in the lower left frame correspond to the result of a conventional threshold scan with three points spaced by 1 GeV , together with the point at $\sqrt{s} = 500 \text{ GeV}$. We note the following:

1. $\Delta = 1 \text{ GeV}$ yields a more precise determination of $m(\tilde{\nu}_e)$ than $\Delta = 30 \text{ GeV}$, especially in row 2, where the luminosity is equally divided between the points. This is a reflection of the fact that it is important to get a good determination of the cross section close to the threshold. In the first row, the difference between the dotted and solid ellipses is small, because most of the luminosity is already spent at the threshold where the cross section is much smaller.
2. As before (and for the same reasons), $m(\tilde{\nu}_e)$ has an asymmetric error with the 90% CL range extending further to the lower side. For an integrated luminosity of 120 fb^{-1} , $m(\tilde{\nu}_e)$ can be determined to lie in a 2 GeV (1.3 GeV) range for Case I (Case II). If an integrated luminosity of 500 fb^{-1} is available, the range shrinks by a factor of about 2.
3. With 120 fb^{-1} of integrated luminosity, the branching fraction for the decay cascade can be determined to better than $\pm 10\%$ for both cases, again with an asymmetric error. The determination of branching fraction and mass are somewhat complementary since the strategy that yields the most precise value of BR yields the largest uncertainty in mass. A data sample of 500 fb^{-1} will reduce the error on the branching fraction by about a factor 2. As in the muon case, the extracted branching ratio must be interpreted with care, since this final state can also arise via other decay chains.

We thus conclude that unless other channels can be included, the sneutrino mass may be determined with a precision of $\sim 0.5\%$, the exact value depending on the branching fraction with an integrated luminosity of 120 fb^{-1} . The precision will about double if an integrated luminosity of 500 fb^{-1} is available.

Since we are talking about a sneutrino mass measurement at the sub-GeV level from counting rate alone, it is necessary to ask whether theoretical uncertainties in the sneutrino production cross section could vitiate such a claim. If this production cross section is uncertain by a considerable amount, this would effectively reflect itself as an increased error in the branching fraction, which would result in a degradation of the mass measurement. As long as the relative error in the cross section remains smaller than that in the branching

that $D \geq 2 \text{ GeV}$, which should be quite feasible since measurements in the continuum will already pin $m(\tilde{\nu}_e)$ with a precision of about 1% [11–13]. This also ensures that our neglect of sneutrino widths does not cause too large an error.

fraction from the error ellipses of Fig. 14, we expect that this will be a subdominant effect, and our previous conclusions will remain valid.

Uncertainties in the cross section could arise due to limitations in our knowledge of masses (or mixing angles) of charginos on which the production cross section depends [25]. We should keep in mind that by the time experiments at LCs are ready to do sub-GeV measurements of $m(\tilde{\nu}_e)$ the mass of \tilde{W}_1 will be determined to better than about 1% [9–13]. We will assume that the heavier chargino mass, assuming (as for the case studies in this paper) $e^+e^- \rightarrow \tilde{W}_1\tilde{W}_2$ production is kinematically accessible, is known with a precision that is no more than five times worse. To understand the impact of these uncertainties in $m(\tilde{W}_1)$ and $m(\tilde{W}_2)$ on the electron sneutrino production cross section, we have computed the change in this cross section by altering $m(\tilde{W}_1)$ and $m(\tilde{W}_2)$ from their nominal values, with the signs of $\Delta m(\tilde{W}_i)$ chosen to maximize this change. We show the fractional uncertainty in the cross section as a function of $\Delta m(\tilde{W}_1)/m(\tilde{W}_1)$ the relative precision with which it is measured, assuming that $\Delta m(\tilde{W}_1)/m(\tilde{W}_1) = 5\Delta m(\tilde{W}_2)/m(\tilde{W}_2)$. The result of our computation of the *maximum* possible change in the cross section (due to mismeasurements of chargino masses) is shown in Fig. 15 for Case I (Case II) by diamonds (triangles) for *a*) $\sqrt{s} = 500$ GeV, and *b*) $\sqrt{s} = 2m(\tilde{\nu}_e) + 2$ GeV. The dot-dashed (dotted) band at 2.7% (4.5%) corresponds to the uncertainty of the cross section due to the uncertainty in the branching ratio (with 500 fb^{-1} of integrated luminosity) from the error ellipses in Fig. 14. We see that as long as the light chargino mass is measured with a precision better than 1.5% (2.5%) in Case I (Case II), the uncertainty from an imperfect knowledge of the chargino masses is smaller than that resulting from the error in the branching fraction in Fig. 14, and our previous conclusions about the precision that would be possible are not greatly altered.

If the heavier chargino is kinematically inaccessible so that $m(\tilde{W}_2)$ cannot be measured, this uncertainty might be larger. For any model with just two charginos, the extreme limit would be $|\mu| \rightarrow \infty$ with M_2 being adjusted to keep $m(\tilde{W}_1)$ within its measured range. In this case, \tilde{W}_1 would be essentially a wino, and the change in the cross section could extend well beyond the band in Fig. 15. Fortunately, by studying chargino pair production we can significantly constrain chargino mixing angles, or equivalently, the $e\tilde{W}_1\tilde{\nu}_e$ coupling [30]. We have not studied whether these constraints from $\tilde{W}_1\tilde{W}_1$ production are sufficiently restrictive for our purpose.

V. CAN WE INCLUDE OTHER CHANNELS?

Up to now, we have confined our analysis to just the $\tau\tau jj\ell$ channel for $\tilde{\nu}_\tau$, and the analogous $\mu\mu jj\ell$ or $eejj\ell$ channels for the other sneutrinos. We remind the reader that for the first channel, the lepton ℓ is defined to be an electron or muon not coming from the decay of a τ . We saw that the precision attained is very sensitive to how close we are able to go to the particle threshold where the signal becomes very small. It is natural to ask whether we can indeed go closer to the threshold by including other channels, and thereby improve the precision.

Clearly, we want to confine ourselves to channels with multiple jets and leptons for which the signal is not obviously overwhelmed by SM backgrounds or by contamination from other SUSY sources. We therefore do not consider direct decays of $\tilde{\nu}_\tau$ to \tilde{Z}_1 since we then have final states with fewer jets/leptons, and hence SM backgrounds and SUSY contamination

much larger than the signal. For $\tilde{\nu}_\tau\tilde{\nu}_\tau$ production, the decay chains that we are left with consist of,

$$\tilde{\nu}_\tau\tilde{\nu}_\tau \rightarrow \tau\widetilde{W}_1\tau\widetilde{W}_1 \rightarrow \tau\tau jj\ell + \cancel{E}_T \quad (1)$$

$$\rightarrow \tau\tau jjjj + \cancel{E}_T \quad (2)$$

$$\rightarrow \tau\tau\ell\ell + \cancel{E}_T \quad (3)$$

$$\tilde{\nu}_\tau\tilde{\nu}_\tau \rightarrow \nu_\tau\widetilde{Z}_2\tau\widetilde{W}_1 \rightarrow \tau jj\ell + \cancel{E}_T \quad (4)$$

$$\rightarrow \tau jjjj + \cancel{E}_T \quad (5)$$

$$\rightarrow \tau\ell^+\ell^-\ell + \cancel{E}_T \quad (6)$$

$$\rightarrow \tau jj\ell^+\ell^- + \cancel{E}_T \quad (7)$$

$$\tilde{\nu}_\tau\tilde{\nu}_\tau \rightarrow \nu_\tau\widetilde{Z}_2\nu_\tau\widetilde{Z}_2 \rightarrow jjjj + \cancel{E}_T \quad (8)$$

$$\rightarrow jj\ell^+\ell^- + \cancel{E}_T \quad (9)$$

$$\rightarrow \ell^+\ell^-\ell^+\ell^- + \cancel{E}_T \quad (10)$$

where we have omitted invisible decays of \widetilde{Z}_2 for the same reason. Muon or electron sneutrino production leads to analogous decay chains that we do not list here.

Channels 8–10 are strongly contaminated by $\tilde{\nu}_e\tilde{\nu}_e$ and $\tilde{\nu}_\mu\tilde{\nu}_\mu$ pair production and also by the production of lighter charginos and neutralinos, so it seems pointless to consider these any further.

We have used ISAJET to compute the cross sections after all cuts and beamstrahlung/ISR corrections in channels 1–7 for both the cases that we have examined. The contributions to each of these channels from the main SUSY sources, along with our estimates of the main $2 \rightarrow 2$ SM backgrounds¹⁵ are shown in Table III for $\sqrt{s} = 500$ GeV. We list separately the contributions from $\tilde{\nu}_\tau\tilde{\nu}_\tau$ production, from the production of the first two generations of sneutrinos and sleptons, from $\tilde{\tau}_1\tilde{\tau}_2 + \tilde{\tau}_2\tilde{\tau}_1$ production (which we separate out because in models with large $\tan\beta$ this can have a threshold that is quite different from the threshold for other sleptons and sneutrinos) and, finally, from the production of chargino and neutralino pairs. There are two entries for the SUSY contributions; the first is for Case I, while the second one (in parenthesis) is for Case II.

We see that channels 4 and 5 have large backgrounds from $t\bar{t}$ production exceeding the signal by a factor of 29 (26) and 173 (67) for Case I (Case II), respectively.¹⁶ While vetoing events with b jets together with top reconstruction cuts may well reduce this background considerably, it will be at some cost to the signal which, in each channel, starts out at a

¹⁵ WWZ production which has a cross section of 4.8 fb is a potential background for some of the event topologies. We do not list its contribution here as we have not simulated these events. We expect though that this contribution is either negligible (as for the $\tau\tau jj\ell$ channel), substantially smaller than other backgrounds listed (as for the $\tau jj\ell$ channel), or easily removeable (as for the $\tau\ell\ell$ channel.)

¹⁶Channel 5 also has an unexpected background of about 1 fb from $W^\pm W^\mp$ production. We have traced this to events where $W \rightarrow q\bar{q}'gg$. This background should be reducible by an invariant mass cut on the $4j$ system, but at some cost to the already small signal.

level of just $\sim 0.1 - 0.25$ fb (0.29 fb) in Case I (Case II). Moreover, the contamination from sleptons and charginos/neutralinos is several times the signal that cuts designed to reconstruct the top background will not significantly reduce.

Channel 3 with the $\tau\tau\ell\ell$ final state has a significant background from ZZ production, though this should be almost eliminated by an invariant mass cut on the $\ell\ell$ system. The bigger problem is that this channel is contaminated by events from SUSY sources: the sleptons, charginos/neutralinos and the staus, each lead to $\tau\tau\ell\ell$ cross sections that exceed the corresponding signal cross section by a factor of 6–8, with $\tilde{\tau}$ events (which would most resemble the signal) contributing about 1/3 (2/3) of the SUSY background.

In channels 6 and 7, although the SM contamination is small, the signal is very tiny. Moreover, the SUSY contamination from the first two generations of sneutrinos and charged sleptons exceeds the signal by a factor of 25-100.

This leaves us with channels 1 and 2. The decays $Z^0 \rightarrow q\bar{q}gg$ result in an unexpected source of SM background in channel 2. The $t\bar{t}$ background, while smaller, is not insignificant. Contamination from chargino/neutralino and stau production is comparable to the signal. While it may well be possible to include this channel at $\sqrt{s} = 500$ GeV, the real problem with this channel comes because we need the same channels in our energy scan. For instance, at an energy 15 GeV above the threshold, the $Z^0 Z^0$ background exceeds the signal by a factor 40 (15) for Case I (Case II), while the top background (present only for Case II) exceeds the signal by a factor ~ 6 . Considering all these problems together with the fact that the signal in Channel 2 would add just 30-50% to Channel 1, we did not think that it was worth including it in our analysis in Sec. IV.

We have also examined whether it might be possible to include other signals from $\tilde{\nu}_\mu\tilde{\nu}_\mu$ to obtain a significantly better determination of $m(\tilde{\nu}_\mu)$. Toward this end, we have computed the cross section in the appropriate channels analogous to those shown in Table III, along with the SM backgrounds. Our results are shown in Table IV for $\sqrt{s} = 500$ GeV. Again the entries in parenthesis refer to the cross sections in Case II. Here, in the last two rows of both the SUSY sources as well as the SM backgrounds, to avoid double counting (with channels 3 and 1), the ℓ in the case of the $\mu\ell\ell\ell$ and $\mu jj\ell\ell$ channels refers only to any e or a μ from the decay of a tau (which, we have assumed, can be tagged by a vertex detector). We should mention that, in this case, for $\ell = \mu$ channel 4 would be the same as channel 9. A similar comment applies *vis à vis* channels 3 and 10. Unfortunately, essentially the same reasoning as before leads us to conclude that it is not possible to improve the sneutrino mass measurement by including other channels.¹⁷

Finally, we turn to the case of electron sneutrinos. As we noted in the last section, the question in this case is whether we can include other channels close to the $\tilde{\nu}_e\tilde{\nu}_e$ threshold so as to be able to cleanly extract the threshold behaviour of the signal cross section. The dominant SUSY contamination at an energy about 2 GeV above the nominal electron sneutrino threshold which mainly comes from the production of charginos and neutralinos is

¹⁷The largest signal is in channel 4. Unfortunately, even if the large top background can be controlled by b -veto and top reconstruction, contamination from other SUSY sources is still large. It may be interesting to see whether it is possible to devise cuts to reduce this background without killing the signal.

shown in Table V along with the $\tilde{\nu}_e$ signal in various channels. In addition, SM backgrounds from W and Z pair production, as well as $t\bar{t}$ production (only for Case II) will also be present. It should be remembered that the cross section for WW production is now very large because $P_L = 0.9$. Backgrounds from $t\bar{t}$ and ZZ production are about 1.5-2 times larger for left polarized electron beams [11]. Channel 5 will have a large background from WW production (see Table IV). For Case II only, $t\bar{t}$ production will be a formidable SM background in channels 4 and 5. In channels 6 and 7, the signal is very small. This leaves us with channels 1-3. Neutralino production (mainly $\tilde{Z}_2\tilde{Z}_2$) contaminates channel 3, particularly in Case II for which it has considerable phase space even at the sneutrino threshold. It is possible, of course, that the signal from sneutrinos may be relatively enhanced by further cuts, *e.g.* on $m(\ell^+\ell^-)$ or $p_T(e)$, but such a detailed analysis is beyond the scope of this study. Finally, we remark that the signal in the remaining (relatively background-free) channel 2 may be combined with that in channel 1 resulting in an increase of about 40%. Presumably, this will increase the precision from that shown in Fig 14 by about 20%.

We should add that in favourable cases, considerably better precision might be possible. For instance, if $t\bar{t}$ production is kinematically forbidden close to the threshold (as in Case I), it should be possible to combine the signal in channel 4 with those in channels 1 and 2, resulting in a three-fold increase in the signal. Optimistically, one may even assume that this may be possible even in Case II since top reconstruction and b -veto may severely reduce the top background. Nonetheless, one sees that even if we combine the signals in all the channels the signal is increased by at most a factor ~ 5 . If we further assume that both SM and SUSY backgrounds can be eliminated without loss of signal, this increased signal is statistically equivalent to an increase in available integrated luminosity. We conclude that even in such a favourable scenario, the precision on $m(\tilde{\nu}_e)$, for an integrated luminosity of $\sim 100 \text{ fb}^{-1}$ will be comparable to that given by the inner ellipse in Fig. 14, but still much larger than the 70 MeV claimed in Ref. [14]. In this case width effects, that we have neglected here, would become important for an analysis of what might be achievable with a data sample of 500 fb^{-1} .

VI. COMMENTS AND CONCLUSIONS

We have performed a detailed examination of the prospects for the determination of sneutrino masses at future linear colliders via a measurement of the energy dependence of the cross section. Threshold studies, which have been claimed [14] to yield a precision better than parts per mille (0.5%) with an integrated luminosity of just 100 fb^{-1} for $m(\tilde{\nu}_e)$ ($m(\tilde{\nu}_\mu)$ and $m(\tilde{\nu}_\tau)$), are a special case of this.

We find that for the second and third generations, the sneutrino production rate leads to less than 1 event for each energy point if we adopt the energy scan strategy and luminosity proposed in Ref. [14] and restrict ourselves to the $\mu\mu jj\ell$ and $\tau\tau jj\ell$ channels that have been suggested to be relatively free of SM backgrounds and SUSY contamination. The availability of 80% positron beam polarization increases the signal by about 40%, but this is not sufficient. Also, including other channels did not appear to help significantly, since in those channels where the signal was substantial, SUSY contamination is also large.

We have also identified a different issue that degrades the precision with which sneutrino masses can be determined from counting experiments, even if the signal is large. The point

is that the size of the signal depends on an unknown branching fraction for sneutrinos to decay to the channel of interest. For sneutrinos, this is a problem of principle because even if backgrounds are small and even with a perfect detector, sneutrinos decaying via $\tilde{\nu} \rightarrow \nu \tilde{Z}_1$ (whose branching fraction can be anything up to 100%) always escape detection. We emphasize that although we are discussing this only in the context of sneutrinos, this issue arises even for charged sparticle mass measurements (except, possibly, for the lightest charged particle as it can only decay to the LSP) in realistic detectors: although SM backgrounds are generally greatly reduced by suitable cuts, to eliminate SUSY contamination, one is frequently forced to study the signal in specific channels whose branching fraction is again to be determined using the same data that is used to extract the mass. Thus, the sparticle mass and this branching fraction have to be simultaneously extracted by fitting both these to the same data. This considerably degrades the precision with which the mass can be determined. While this is, in principle, also a problem for the extraction of masses using kinematic strategies [9–13], the sensitivity to the unknown branching fraction is presumably smaller.

For sparticles whose cross sections into channels where SUSY contamination and SM backgrounds are under control is relatively small, we found that the following offers a reasonable strategy for extracting their mass:

- Use about 15-20% of the available integrated luminosity at the nominal collider energy which, we assume is well beyond the sneutrino production threshold. In our analysis, we took this to be 500 GeV. A measurement of the cross section at this energy strongly constrains the branching fraction.
- Divide the remaining integrated luminosity to measure the cross section at about three additional lower energy points in such a manner so as to obtain about an equal number of events at each point so that the fractional error in the cross section at each energy is about the same. Since the precision on the mass improves if we are able to go close to the threshold where the cross section is small and a large integrated luminosity is required to get a fixed number of events, we found that it was best to space these points $\Delta \sim 60$ GeV apart. This is because two of the three points are away from the threshold and so can reach the target number of events with a modest integrated luminosity.

Specifically, for muon and tau type sneutrinos, the availability of right-handed electron beams was essential to reduce the contamination from electron sneutrinos and chargino production. We made several optimistic assumptions for our analysis. First, we assumed that 95% electron beam polarization will be available. Second, for the determination of $m(\tilde{\nu}_\tau)$, we assumed that vertex detection would allow leptonically decaying taus to be tagged with an efficiency close to 100%. While this would also allow hadronically decaying taus to be discriminated from light quark and gluon jets, the need to discriminate tau jets from c -jets required us to impose requirements on hadronically decaying taus that reduce their efficiency, but maintain the purity of the tau sample. We should, however, remind the reader that we have used the beamstrahlung spectrum appropriate to $\sqrt{s} = 500$ GeV all the way down to the sneutrino mass threshold. This will cause us to somewhat underestimate the precision that might be attained.

Even so, we found that an integrated luminosity of 100 fb^{-1} was too small for a measurement of $m(\tilde{\nu}_\tau)$. This is because we were forced to confine our analysis to the cleanest $\tau\tau jj\ell$ channel. Other channels either had small cross sections or suffered from considerable SUSY backgrounds. A crude determination of $m(\tilde{\nu}_\mu)$ may be possible¹⁸ at least in Case II even with an integrated luminosity of $\sim 100 \text{ fb}^{-1}$, but since $m(\tilde{\nu}_\mu)$ and $m(\tilde{\nu}_\tau)$ can be determined via essentially the same collider runs, we have assumed an integrated luminosity of 500 fb^{-1} for both analyses. Even then, we found that, at best, a measurement of these masses with a precision of several percent (at 90% CL) is possible, with of course $m(\tilde{\nu}_\mu)$ being 2–3 times better determined than $m(\tilde{\nu}_\tau)$. The exact precision that can be attained depends on the branching fraction into the useful channels which can vary by a factor 2–3 for representative ranges of SUSY parameters.¹⁹ The attainable precision will also depend to some extent on how well SUSY backgrounds may be controlled. The main results of our studies are shown in Fig. 10 for $\tilde{\nu}_\tau$ and Fig. 13 for $\tilde{\nu}_\mu$, and summarized in Table VI. We emphasize again that these results are for a model-independent analysis. As discussed in Sec. IVC, analyses within particular frameworks such as mSUGRA may yield much higher precision.

It also seems worthwhile to stress that unlike a closely spaced threshold scan the strategy of taking data at widely spaced intervals would conceivably be useful for other physics, than just sneutrino masses. For instance, the same energy scan could be used to simultaneously obtain masses of several sparticles or even make measurements useful for Higgs boson, top as well as electroweak or QCD studies.

We also examined prospects for determining $m(\tilde{\nu}_e)$. For this, of course, left-handed electron polarization is optimal. Again, it appeared to be best to use about 20% of the available luminosity at the nominal energy, and divide the remainder among about three points at lower energies with equal number of events at each point. In contrast to the second and third generation cases, it seemed best to choose the points just about 1 GeV apart, though the precision for a 30 GeV spacing is not much worse as can be seen in the first row of Fig. 14. Indeed the consideration in the previous paragraph may suggest that this may be better for the overall physics program at the LC. The reader should keep in mind that even with this strategy most of the data will be at the one point closest to the threshold. With an integrated luminosity of 120 fb^{-1} , a precision of about 0.5% (90% CL) appears to be possible. This will improve by a factor 2 for a data sample of 500 fb^{-1} . In this case, some improvement may be possible by combining several channels. The dotted ellipses in the second row show that the precision on $m(\tilde{\nu}_e)$ will be degraded by about 25-30% if, in the interest of the overall LC program, it is decided to collect equal amounts of integrated luminosity at points spaced 30 GeV apart.

To conclude, we reiterate that experiments at the LC will be able to determine masses of sneutrinos with significant precision but certainly for the third generation, and possibly also second generation, sneutrino mass determination an integrated luminosity $\sim 500 \text{ fb}^{-1}$ seems essential. However, even with this large luminosity, the precision claimed in Ref. [14] does not

¹⁸Fig. 12 allows the reader to assess how small D can be to maintain the six event minimum as we have required.

¹⁹Of course, there are regions of parameter space where the variation may be outside this range.

seem possible. While we have not checked this, the mass resolution for the heavier charged sleptons $\tilde{\mu}_L$ and $\tilde{\tau}_2$ is presumably not any better than that for the corresponding sneutrinos. The masses of first generation sneutrinos can be determined with much greater precision, but even in this case, our projections for the precision are nowhere near as optimistic as those in Ref. [14]. We caution that several beautiful analyses [14,17,31] about what might be attainable in light of measurements at a LC might be painting too rosy a picture.

ACKNOWLEDGMENTS

We thank G. Blair and H.-U. Martyn for communications at the early stages of this study. We are grateful to R.M. Godbole for her continuing interest, and for comments on an early draft of this paper. This research was supported in part by the U. S. Department of Energy under contract number DE-FG02-97ER41022 and DE-FG-03-94ER40833.

REFERENCES

- [1] *Electroweak Symmetry Breaking and New Physics at the TeV Scale* T. Barklow, S. Dawson, H. Haber and J. Siegrist, Editors (World Scientific, 1996).
- [2] *New Directions for High Energy Physics*, Snowmass 96 Summer Study, D. Cassel, L. Trindle Gennari and R.H Siemann, Editors (SLAC, 1997).
- [3] ATLAS Technical Design Report, CERN/LHCC/99-14 (1999)
- [4] CMS Technical Proposal, CERN/LHCC/94-38 (1994); S. Abdullin *et al.*, hep-ph/9806366 (1998).
- [5] A. Bartl *et al.* Ref. [2].
- [6] I. Hinchliffe, F. Paige, M. Shapiro, J. Söderqvist and W. Yao, Phys. Rev D **55**, 5520 (1997).
- [7] I. Hinchliffe and F. Paige, Phys. Rev. D **60**, 095002 (1999).
- [8] S. Ambrosanio, B. Mele, S. Petrarca, G. Polesello and A. Rimoldi, J. High Energy Phys. **0101**, 014 (2001).
- [9] JLC-1, KEK Report No. 92-16 (1992) (unpublished).
- [10] T. Tsukamoto *et al.*, Phys. Rev. D **51**, 3153 (1995).
- [11] H. Baer, R. Munroe and X. Tata, Phys. Rev. D **54**, 6735 (1996).
- [12] S. Kuhlman *et al.* NLC Zero Design Report, SLAC Report 485 (1996).
- [13] M. Danielson *et al.*, Ref. [2].
- [14] G.A. Blair and H.-U. Martyn, hep-ph/9910416 (1999); TESLA Technical Design Report, DESY 2001-011 (2001).
- [15] S. Ambrosanio and G. A Blair, Eur. Phys. J. **C12**, 287 (2000).
- [16] P. G. Mercadante, J. K. Mizukoshi and H. Yamamoto, Phys. Rev. D **64**, 015005 (2001).
- [17] G.A. Blair, W. Porod, P.M. Zerwas, Phys. Rev. D **63**, 017703 (2001).
- [18] H. Baer, C. Balázs, S. Hesselbach, J. K. Mizukoshi, X. Tata, Phys. Rev. D **63**, 095008 (2001).
- [19] M. Schmaltz and W. Skiba, Phys. Rev. D **62**, 095005 (2000); *ibid* **62**, 095004 (2000). For earlier ideas, see D. Kaplan, G. Kribs and M. Schmaltz, Phys. Rev. D **62**, 035010 (2000); Z. Chacko, M. Luty, A. Nelson and E. Ponton, J. High Energy Phys. **01**, 003 (2000).
- [20] H. Baer, C. Balázs, J. K. Mizukoshi, X. Tata, Phys. Rev. D **63**, 055011 (2001).
- [21] P. Igo-Kemenes, invited talk at the *International Conference on High Energy Physics*, 2000, Osaka, Japan (to appear in the Proceedings).
- [22] H. Brown *et al.* (Muon $g - 2$ Collaboration), Phys. Rev. Lett. **86**, 2227 (2001).
- [23] F. Paige, S. Protopopescu, H. Baer and X. Tata, hep-ph/0001086 (2000).
- [24] O. J. P. Éboli, M. C. Gonzales-Garcia, J. K. Mizukoshi, Phys. Rev. D **58**, 034008 (1998).
- [25] J. Feng and M. Peskin, hep-ph/0105100 (2000).
- [26] H.-U. Martyn, hep-ph/0002290 (2000).
- [27] M. Peskin, Linear Collider Collaboration technical note LCC-0010 (1999) and references therein.
- [28] M. Skrzypek and S. Jadach, Z. Phys. **C49**, 577 (1991).
- [29] See http://www-project.slac.stanford.edu/lc/local/AccelPhysics/Accel_Physics_index.htm.

- [30] J. Feng, M. Peskin, H. Murayama and X. Tata, Phys. Rev. D **52**, 1418 (1995); H-C. Cheng, J. Feng and N. Polonsky, Phys. Rev. D **57**, 152 (1998); S. Kiyoura, M. Nojiri, D. Pierce and M. Peskin, Phys. Rev. D **58**, 075002 (1998).
- [31] S.Y. Choi, A. Djouadi, M. Guchait, J. Kalinowski, H.S. Song and P.M. Zerwas, Eur. Phys. J. **C14**, 535 (2000).

TABLES

TABLE I. Relevant sparticle masses in GeV and branching fractions for Case I and Case II introduced in Sec. I of the text. The last line shows the branching fraction into the relatively background free $\tau\tau jj\ell$ channel discussed in Sec. II.

	Case I	Case II
$m(\tilde{e}_R)$	130.4	167.8
$m(\tilde{e}_L)$	173.7	194.2
$m(\tilde{\nu}_e)$	158.3	178.3
$m(\tilde{\tau}_1)$	129.3	165.7
$m(\tilde{\tau}_2)$	174.4	195.4
$m(\tilde{\nu}_\tau)$	158.3	178.1
$m(\tilde{W}_1)$	128.9	105.6
$m(\tilde{W}_2)$	340.2	283.4
$m(\tilde{Z}_1)$	72.0	59.9
$m(\tilde{Z}_2)$	131.4	108.2
$m(\tilde{Z}_3)$	313.5	255.5
$m(\tilde{Z}_4)$	343.0	284.3
m_h	99.4	105.0
m_A	366.1	310.5
μ	309.7	248.4
$B(\tilde{\nu}_\tau \rightarrow \tau\tilde{W}_1)$	0.37	0.56
$B(\tilde{W}_1 \rightarrow \ell\nu\tilde{Z}_1)$	0.154	0.124
$B(\tilde{W}_1 \rightarrow q\bar{q}\tilde{Z}_1)$	0.523	0.626
$B(\tilde{\nu}_\tau\tilde{\nu}_\tau \rightarrow \tau\tau jj\ell)$	0.044	0.097

TABLE II. The cross section after cuts for the $\tau\tau jj\ell$ signal at $\sqrt{s} = 500$ GeV for several channels for the two cases discussed in the text. Here j^τ and ℓ^τ refer to a jet or lepton (e or μ) from the decay of a tau, which itself is produced via the decay of a heavy particle. The parameter r_{min} which is used to discriminate between τ and c jets has been introduced in Sec. IV. We see that if the taus can be tagged via their leptonic decay, the signal is more than doubled.

topology	r_{min}	σ^{obs} (fb) (Case I)	σ^{obs} (fb) (Case II)
$2j^\tau + 2j^{QCD} + \ell + \cancel{E}_T$	0.5	0.045	0.118
	0.8	0.040	0.114
	1.0	0.028	0.094
$j^\tau + \ell^\tau + 2j^{QCD} + \ell + \cancel{E}_T$	0.5	0.051	0.130
	0.8	0.047	0.129
	1.0	0.039	0.119
$\ell^\tau + \ell^\tau + 2j^{QCD} + \ell + \cancel{E}_T$	-	0.015	0.033

TABLE III. The cross section in fb after all the cuts but no beamstrahlung/ISR corrections for channels 1–7 discussed in Sec. V of the text from several SUSY sources along with SM backgrounds at $\sqrt{s} = 500$ GeV. The first of the SUSY contributions is for Case I while the second one (in parenthesis) is for Case II.

SUSY SOURCES				
Channel	$\tilde{\nu}_\tau \tilde{\nu}_\tau$	$\tilde{l}_L, \tilde{\nu}_\ell$	\tilde{W}_i, \tilde{Z}_j	$\tilde{\tau}_1, \tilde{\tau}_2$
$\tau\tau jj\ell$	0.110 (0.281)	0.049 (0.182)	0.054 (0.159)	0.024 (0.027)
$\tau\tau jjjj$	0.033 (0.144)	0.000 (0.000)	0.030 (0.145)	0.002 (0.091)
$\tau\tau\ell\ell$	0.088 (0.164)	0.363 (0.430)	0.080 (0.224)	0.240 (0.622)
$\tau jj\ell$	0.258 (0.291)	1.24 (1.34)	1.08 (0.774)	0.463 (0.296)
$\tau jjjj$	0.113 (0.293)	0.005 (0.001)	0.616 (1.15)	0.040 (0.379)
$\tau\ell\ell\ell$	0.012 (0.049)	1.50 (1.39)	0.099 (0.145)	0.074 (0.092)
$\tau jj\ell\ell$	0.007 (0.043)	0.667 (1.25)	0.069 (0.184)	0.045 (0.092)

SM BACKGROUNDS			
Channel	$W^\pm W^\mp$	$Z^0 Z^0$	$t\bar{t}$
$\tau\tau jj\ell$	0.000	0.002	0.003
$\tau\tau jjjj$	0.000	0.098	0.068
$\tau\tau\ell\ell$	0.000	0.557	0.000
$\tau jj\ell$	0.006	0.001	7.57
$\tau jjjj$	1.17	0.063	19.5
$\tau\ell\ell\ell$	0.000	0.000	0.000
$\tau jj\ell\ell$	0.000	0.000	0.011

TABLE IV. The same as Table III but for channels with potential signals from $\tilde{\nu}_\mu$ production. For the $\mu\ell\ell\ell$ and $\mu jj\ell\ell$ channels, the ℓ refers to any electron or a muon from tau decay. This avoids double counting as discussed in the Sec. V of the text.

SUSY SOURCES			
Channel	$\tilde{\nu}_\mu\tilde{\nu}_\mu$	$\tilde{l}_L, \tilde{\nu}_\ell$	\tilde{W}_i, \tilde{Z}_j
$\mu\mu jj\ell$	0.288 (0.539)	0.177 (0.451)	0.118 (0.276)
$\mu\mu jjjj$	0.084 (0.244)	0.002 (0.149)	0.050 (0.225)
$\mu\mu\ell\ell$	0.264 (0.341)	1.21 (1.16)	0.139 (0.380)
$\mu jj\ell$	0.506 (1.06)	2.45 (2.89)	1.58 (2.01)
$\mu jjjj$	0.113 (0.298)	0.106 (0.501)	0.927 (1.54)
$\mu\ell\ell\ell$	0.009 (0.020)	1.07 (1.20)	0.047 (0.070)
$\mu jj\ell\ell$	0.007 (0.031)	0.822 (1.74)	0.057 (0.141)

SM BACKGROUNDS			
Channel	$W^\pm W^\mp$	$Z^0 Z^0$	$t\bar{t}$
$\mu\mu jj\ell$	0.000	0.000	0.003
$\mu\mu jjjj$	0.000	0.001	0.122
$\mu\mu\ell\ell$	0.000	0.039	0.000
$\mu jj\ell$	0.001	0.317	8.17
$\mu jjjj$	1.35	0.001	23.0
$\mu\ell\ell\ell$	0.000	0.000	0.000
$\mu jj\ell\ell$	0.000	0.001	0.000

TABLE V. The cross section in fb for potential signals from $\tilde{\nu}_e\tilde{\nu}_e$ production at $\sqrt{s} = 320$ GeV (360 GeV) along with chargino and neutralino contamination for Case I (Case II). In this table, $P_L = 0.9$. For the $elll$ and $ejjll$ channels, the ℓ refers to any muon or a electron from tau decay. This is to avoid double counting.

Channel	$\tilde{\nu}_e\tilde{\nu}_e$	\tilde{W}_i, \tilde{Z}_j
$eejjl$	0.233 (0.533)	0 (0)
$eejjjj$	0.080 (0.207)	0 (0)
$eell$	0.247 (0.420)	0.225 (1.68)
$ejjl$	0.514 (1.45)	0.188 (6.59)
$ejjjj$	0.111 (0.276)	0.013 (0.040)
$elll$	0.004 (0.023)	0 (0)
$ejjll$	0.004 (0.027)	0 (0)

TABLE VI. A summary of our projections for sneutrino mass measurements (90% CL) in Case I and Case II, assuming a 95% longitudinally polarized beam. For especially $\tilde{\nu}_\tau$, a significant mass measurement does not appear to be possible with 100 fb^{-1} . For each of $m(\tilde{\nu}_\tau)$ and $m(\tilde{\nu}_\mu)$, the first row shows our projection with backgrounds and SUSY contamination as discussed in the text, while the next one shows the corresponding projection if these backgrounds can be effectively eliminated without loss of signal. For $\tilde{\nu}_e$, both SM background and SUSY contamination are insignificant.

	Case I	Case II
$m(\tilde{\nu}_\tau)$ (500 fb^{-1})	$153^{+12.5}_{-24}$ GeV	$174.9^{+7.1}_{-15.4}$ GeV
	$153^{+11.5}_{-24}$ GeV	$175.4^{+5.6}_{-10.9}$ GeV
$m(\tilde{\nu}_\mu)$ (500 fb^{-1})	$156.4^{+4.2}_{-7.9}$ GeV	$175.7^{+3.9}_{-4.6}$ GeV
	$156.4^{+4.1}_{-7.4}$ GeV	$176.4^{+3.3}_{-5.2}$ GeV
$m(\tilde{\nu}_e)$ (120 fb^{-1})	$157.8^{+0.8}_{-1.2}$ GeV	$178.0^{+0.5}_{-0.8}$ GeV
$m(\tilde{\nu}_e)$ (500 fb^{-1})	$158.1^{+0.4}_{-0.5}$ GeV	$178.2^{+0.2}_{-0.4}$ GeV

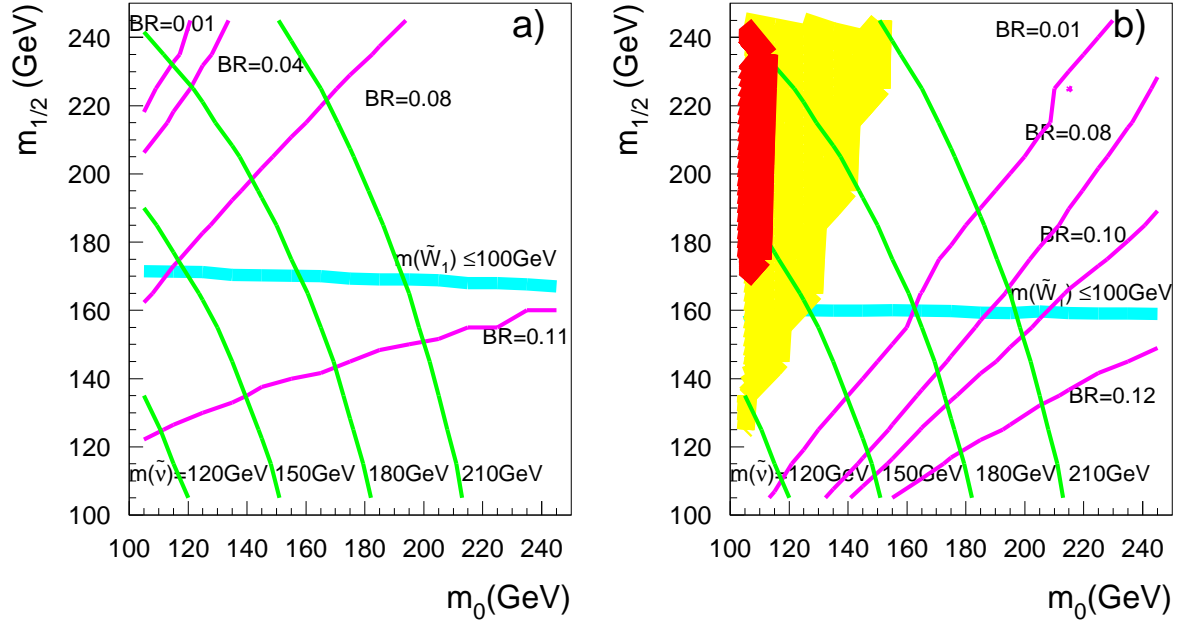


FIG. 1. Contours of the branching ratio $\tilde{\nu}_\tau \tilde{\nu}_\tau \rightarrow \tau \tilde{W}_1 \tau \tilde{W}_1 \rightarrow \tau \tau j j + \ell + \cancel{E}_T$ for a) $\tan \beta = 3$ and b) $\tan \beta = 40$. Also shown are contours of $m(\tilde{\nu}_\tau)$. In the region below the thick line, $m(\tilde{W}_1) \leq 100$ GeV, roughly the lower limit on the chargino mass from LEP experiments. The dark (light) shaded regions in frame b) are excluded because $m^2(\tilde{\tau}_R) < 0$ ($\tilde{\tau}_1$ is the LSP).

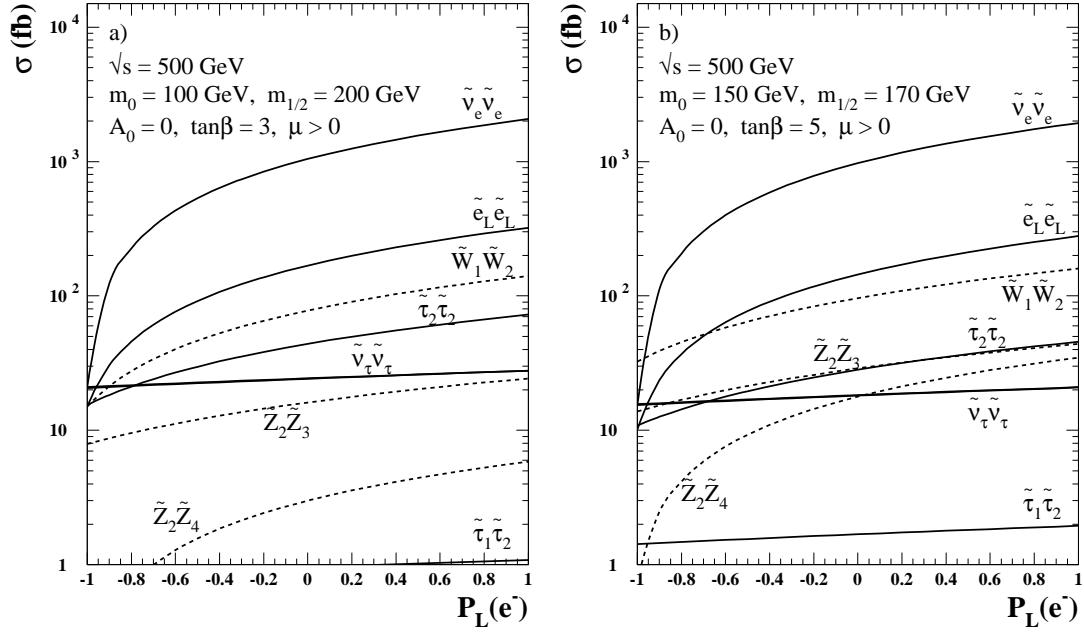


FIG. 2. Production cross sections for several SUSY processes at a $\sqrt{s} = 500$ GeV e^+e^- collider versus the electron beam polarization parameter $P_L(e^-)$. The solid (dashed) lines are the cross sections for various slepton and sneutrino (chargino and neutralino) pair production processes. Frame *a*) is for Case I and frame *b*) is for Case II.

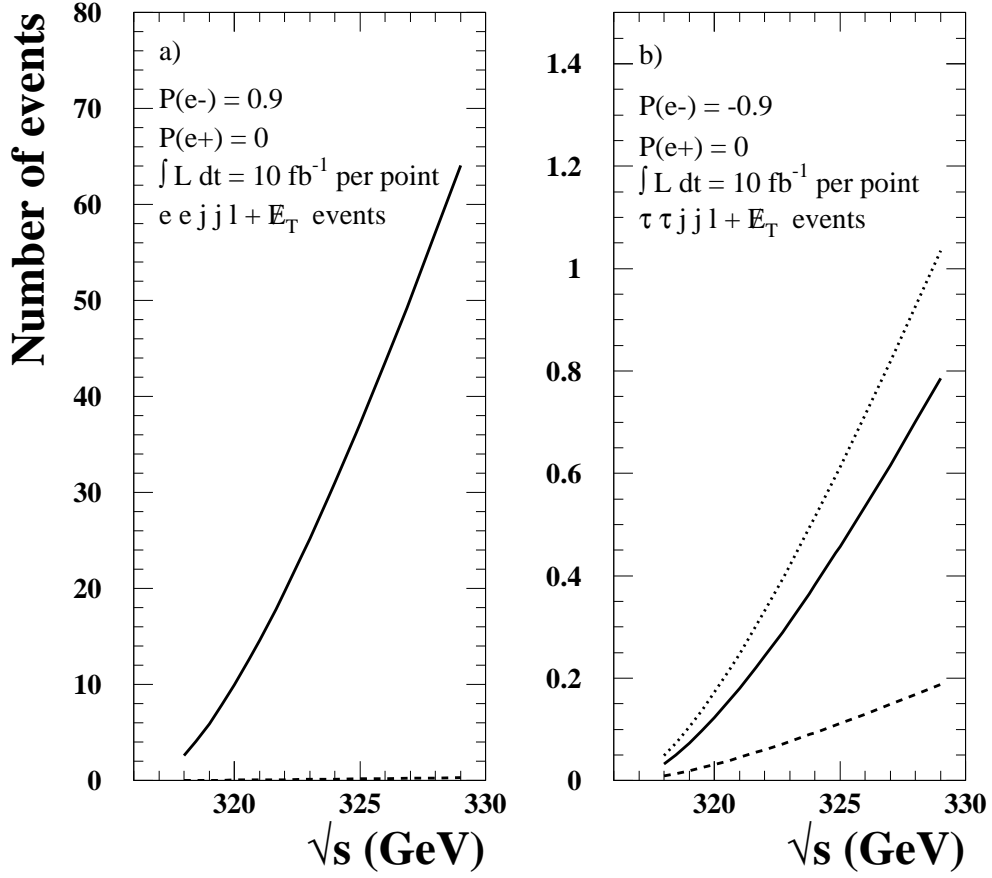


FIG. 3. An illustration of event rates close to the sneutrino production threshold for Case I. In frame *a*) we show the rate in the favoured $eejj\ell$ channel from $\tilde{\nu}_e\tilde{\nu}_e$ production with $P_L(e^-) = 0.9$. The dashed line shows the contamination from $\tilde{\nu}_\mu\tilde{\nu}_\mu$ production. In frame *b*), we show rates for the corresponding $\tau\tau jj\ell$ channel from $\tilde{\nu}_\tau\tilde{\nu}_\tau$ production, but with $P_L(e^-) = -0.9$ (dotted line) along with contamination from $\tilde{\nu}_e\tilde{\nu}_e$ production (solid line) and $\tilde{\nu}_\mu\tilde{\nu}_\mu$ production (dashed line). In both frames we have assumed that the integrated luminosity is 10 fb^{-1} for each energy point.

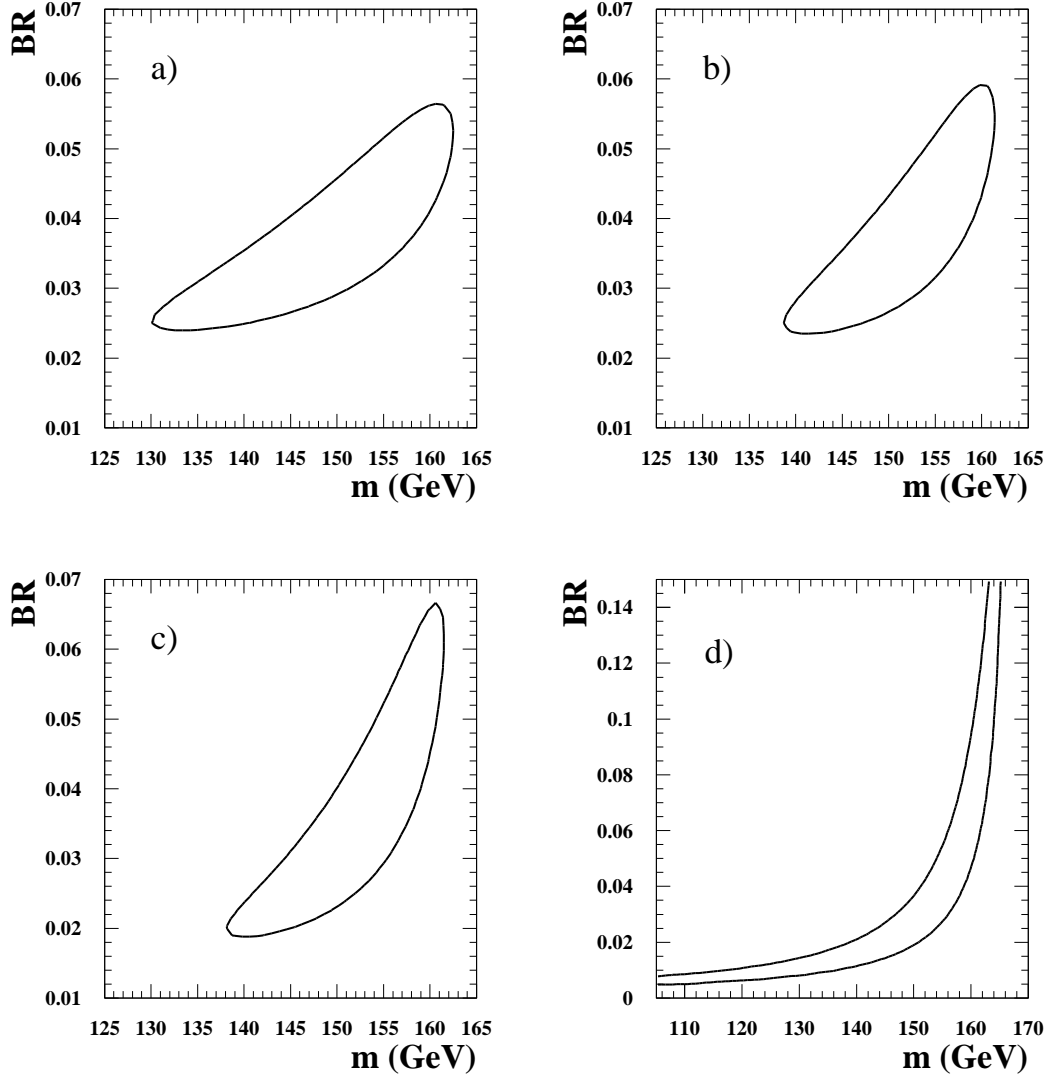


FIG. 4. 90% CL ($\Delta\chi^2 = 4.6$) contours for a fixed 10 events per point (for the input theory) at lower energies, with $N = 3$ and $\Delta = 5$ GeV. In a) $\mathcal{L}_{low} = 60 \text{ fb}^{-1}$, $\mathcal{L}_0 = 60 \text{ fb}^{-1}$ and $D = 45$ GeV; in b) $\mathcal{L}_{low} = 80 \text{ fb}^{-1}$, $\mathcal{L}_0 = 40 \text{ fb}^{-1}$ and $D = 32$ GeV; in c) $\mathcal{L}_{low} = 100 \text{ fb}^{-1}$, $\mathcal{L}_0 = 20 \text{ fb}^{-1}$ and $D = 26$ GeV, and in d) $\mathcal{L}_{low} = 120 \text{ fb}^{-1}$, $\mathcal{L}_0 = 0 \text{ fb}^{-1}$ and $D = 21$ GeV. The analysis is with the parameters of Case I.

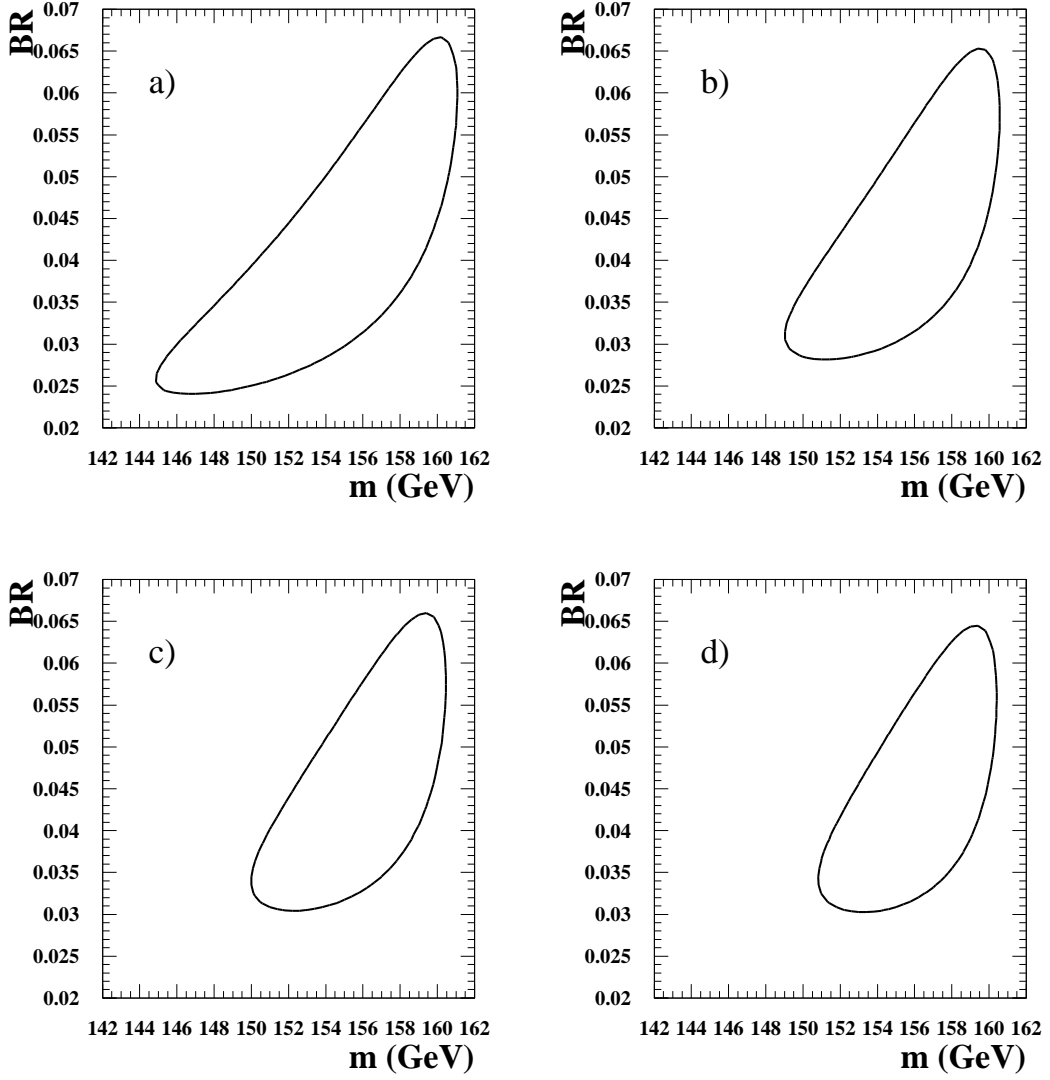


FIG. 5. 90% CL ($\Delta\chi^2 = 4.6$) contours for a fixed 10 events per point (for the input theory) at lower energies, with $N = 3$, $\mathcal{L}_{low} = 100 \text{ fb}^{-1}$ and $\mathcal{L}_0 = 20 \text{ fb}^{-1}$. In a) $\Delta = 20 \text{ GeV}$ and $D = 19 \text{ GeV}$; in b) $\Delta = 40 \text{ GeV}$ and $D = 16 \text{ GeV}$; in c) $\Delta = 60 \text{ GeV}$ and $D = 16 \text{ GeV}$, and in d) $\Delta = 80 \text{ GeV}$ and $D = 15 \text{ GeV}$. The analysis is with the parameters of Case I.

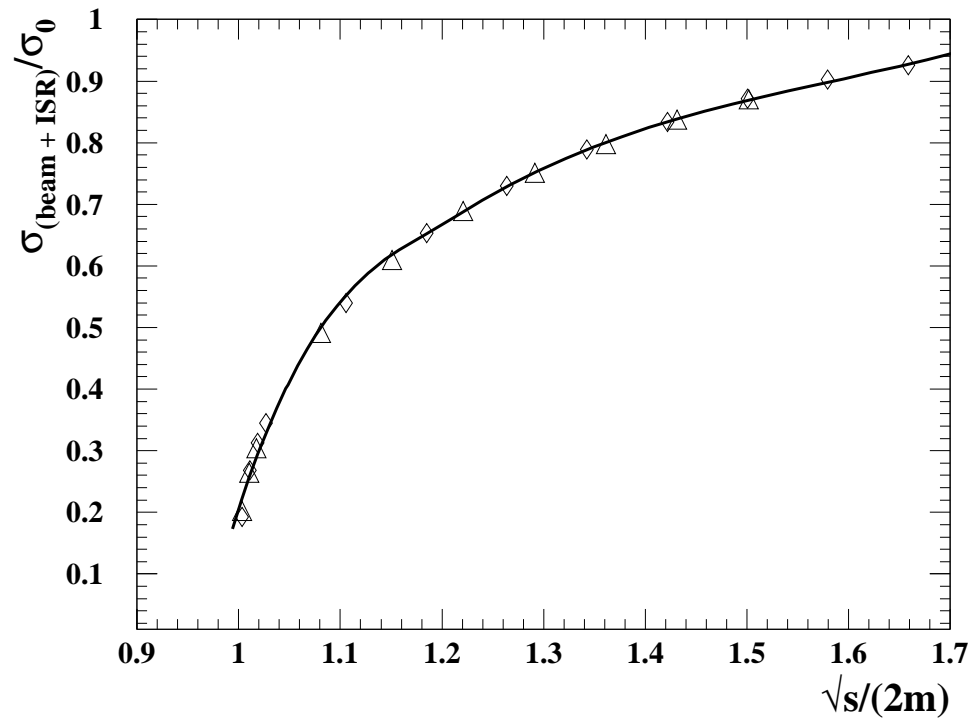


FIG. 6. Ratio of $\tilde{\nu}_\tau$ (or $\tilde{\nu}_\mu$) pair production cross sections with and without initial state radiation and beamstrahlung effects versus the center of mass energy divided by the sum of sneutrino masses. Diamonds (squares) denote the results for Case I (II).

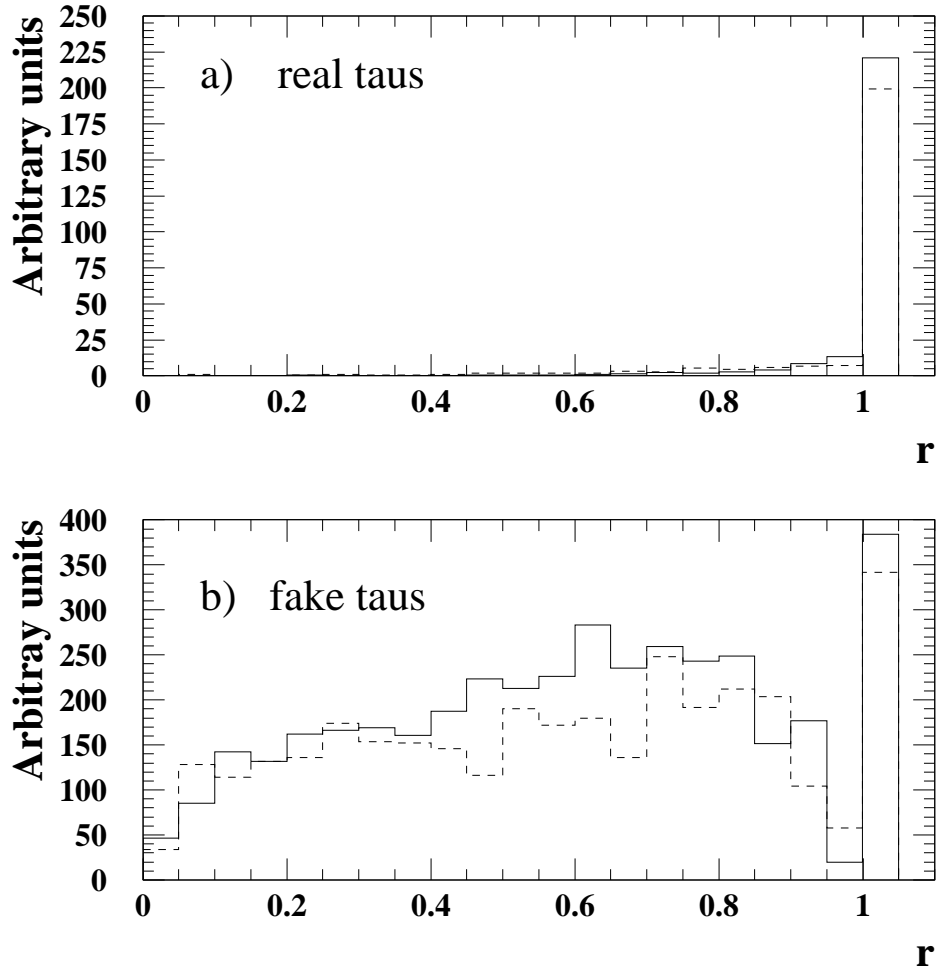


FIG. 7. The rate for *a)* real and *b)* fake tau jets versus the $\tau - c$ discrimination parameter r defined in Eq. (3) of the text. The dashed histogram shows the result for Case I, while the solid histogram shows the corresponding result for Case II.

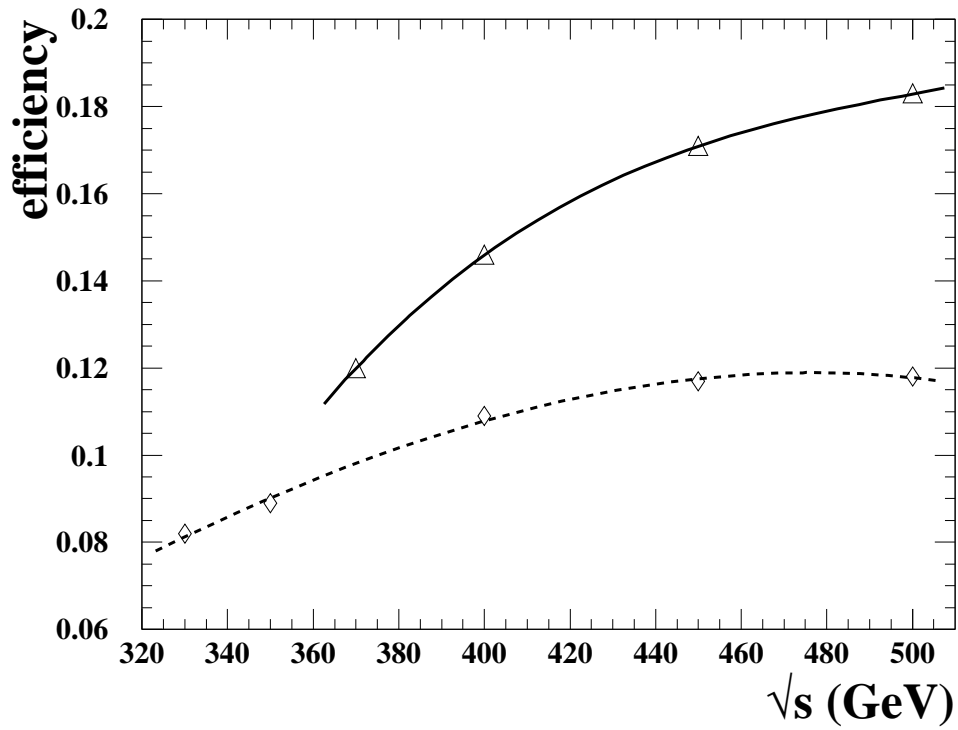


FIG. 8. Reconstruction efficiency for the $\tau\tau jj\ell + E_T$ channel in Case I (diamonds) and II (triangles). The solid and dashed lines show the fitted efficiency functions that we use in our analysis.

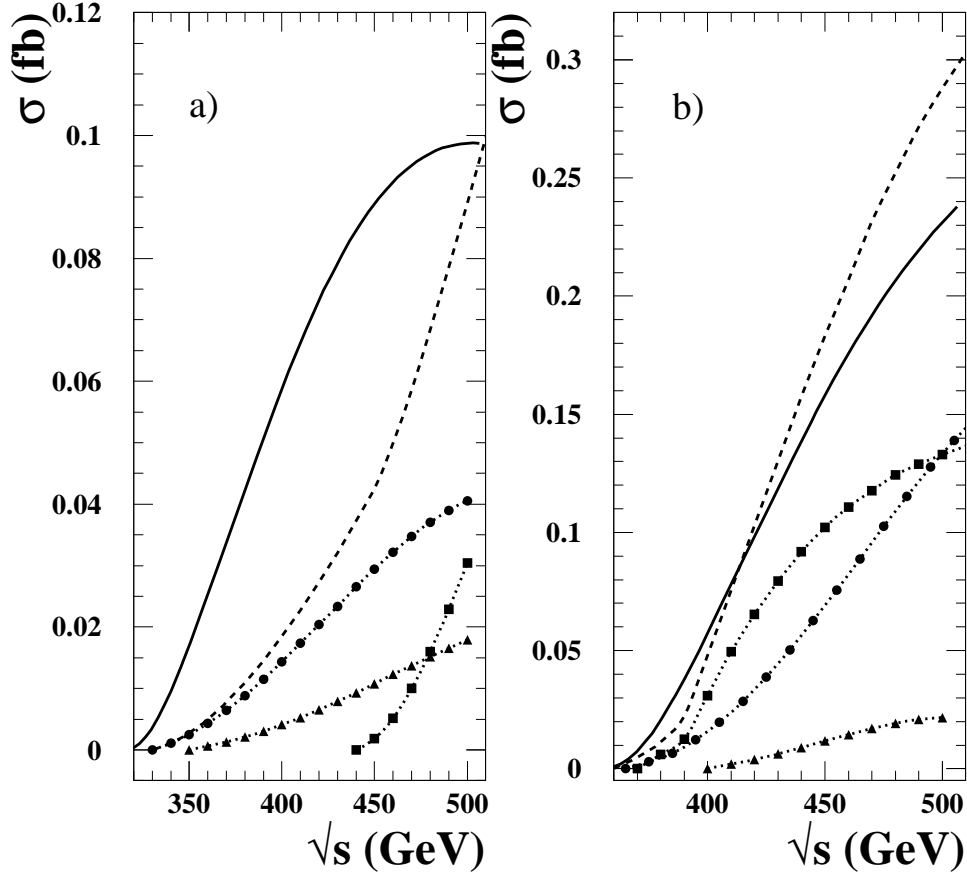


FIG. 9. Signal (solid line) and the total SUSY background (dashed line) cross sections for $\tau\tau jj\ell + \cancel{E}_T$ after including the effects of ISR and beamstrahlung, as well as the reconstruction efficiency, versus the center of mass energy. The circles, squares and triangles show SUSY contamination from first two generations of charged sleptons and sneutrinos, charginos and neutralinos, and $\tilde{\tau}_1\tilde{\tau}_2 + \tilde{\tau}_2\tilde{\tau}_1$ production, respectively. The dotted line is the fit to these component backgrounds that we use in our analysis. Frame *a*) is for Case I while frame *b*) is for Case II.

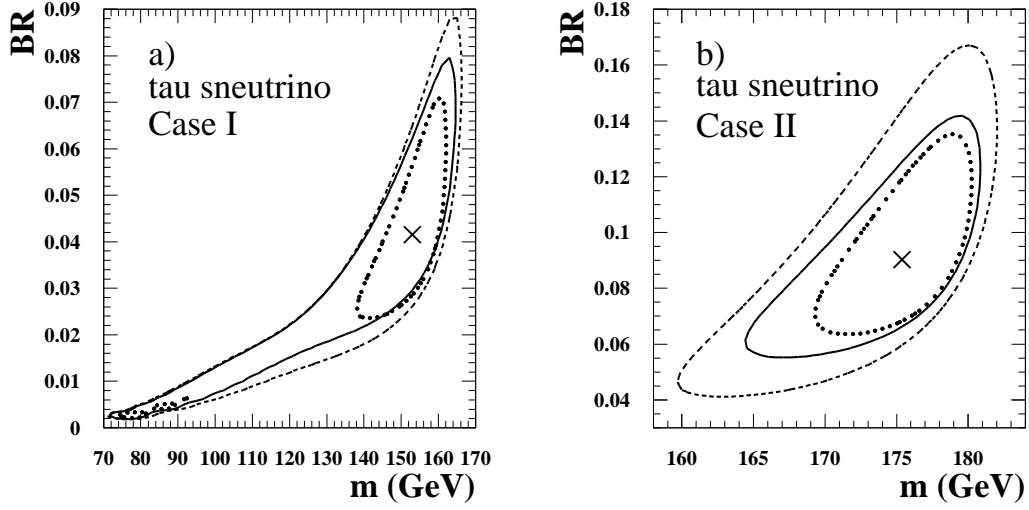


FIG. 10. 90% CL ($\Delta\chi^2 = 4.6$) contours for a fixed 6 events per point (for the input theory) at lower energies, with $N = 3$, $\mathcal{L}_{low} = 400 \text{ fb}^{-1}$, $\mathcal{L}_0 = 100 \text{ fb}^{-1}$, and $\Delta = 60 \text{ GeV}$. In both frames the solid (dashed) line stands for limits without (with) SUSY backgrounds, while the dotted line shows how much the error ellipse shrinks for an integrated luminosity 1.5 times higher, assuming no background. The cross inside the ellipses shows the best fitted point. Frame *a*) shows the result for Case I and has $D = 42$ (30) GeV for the solid and dashed (dotted) ellipses, while frame *b*) which is for Case II, has $D = 23$ (18) GeV for the solid and dashed (dotted) ellipse. The cross shows the best fit.

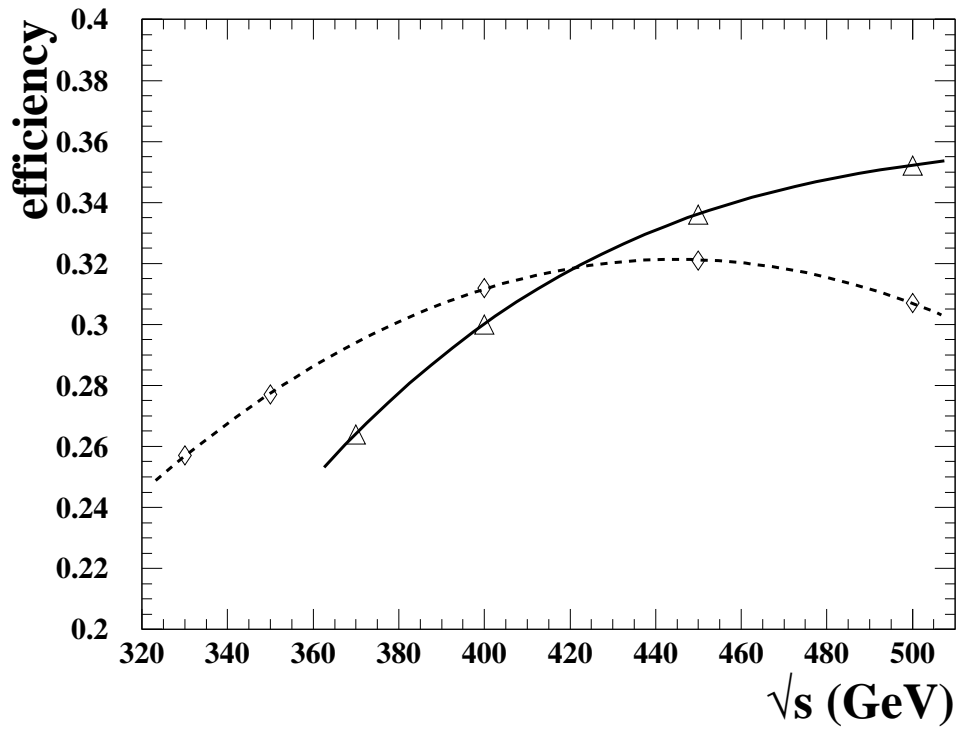


FIG. 11. Same as in Fig. 8 but for the $\mu\mu jj\ell + \cancel{E}_T$ channel.

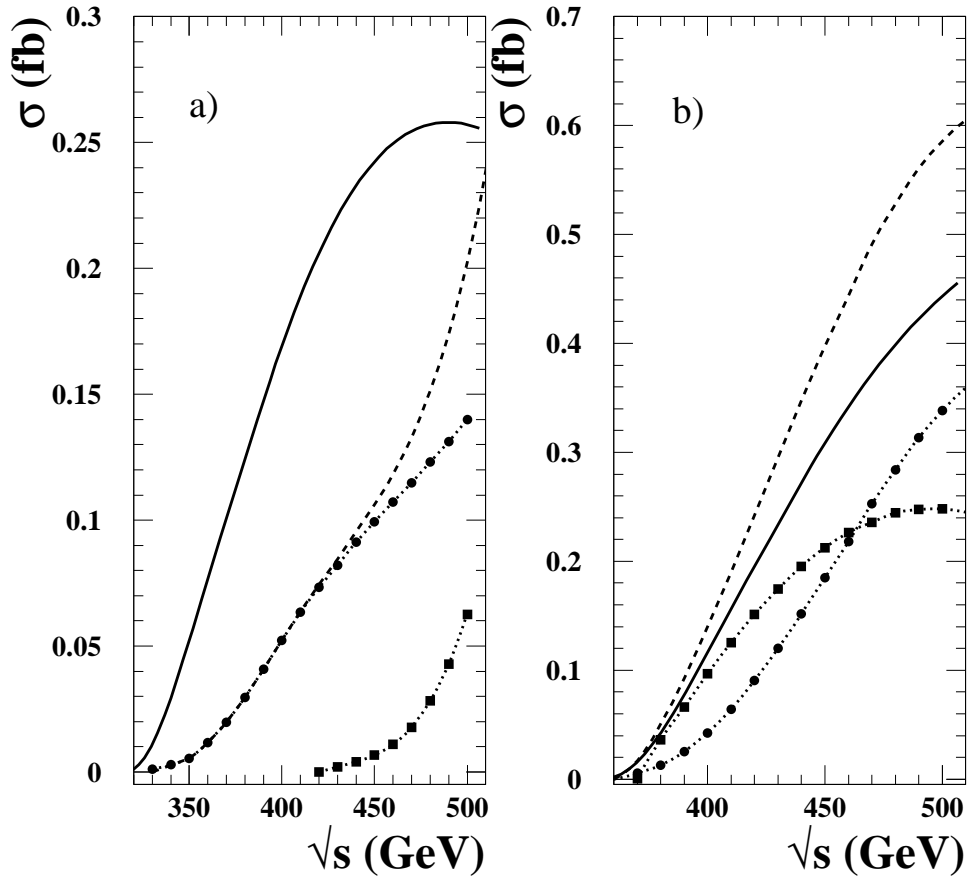


FIG. 12. Same as in Fig. 9 for the $\mu\mu jj\ell + \cancel{E}_T$ events, except that the circles include contamination from all charged sleptons including smuons.

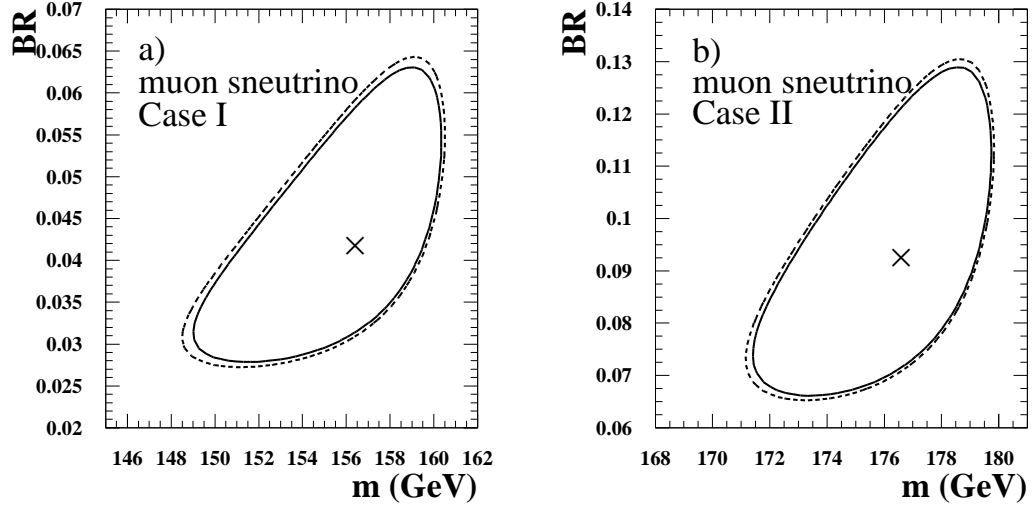


FIG. 13. 90% CL ($\Delta\chi^2 = 4.6$) contours for a fixed 6 events per point (for the input theory) at lower energies, with $N = 3$, $\mathcal{L}_{low} = 400 \text{ fb}^{-1}$, $\mathcal{L}_0 = 100 \text{ fb}^{-1}$, and $\Delta = 60 \text{ GeV}$. In both frames the solid (dashed) line stands for limits without (with) SUSY backgrounds. In a) the result is for Case I, with $D = 18 \text{ GeV}$, and in b) Case II, with $D = 14 \text{ GeV}$. The cross shows the best fit.

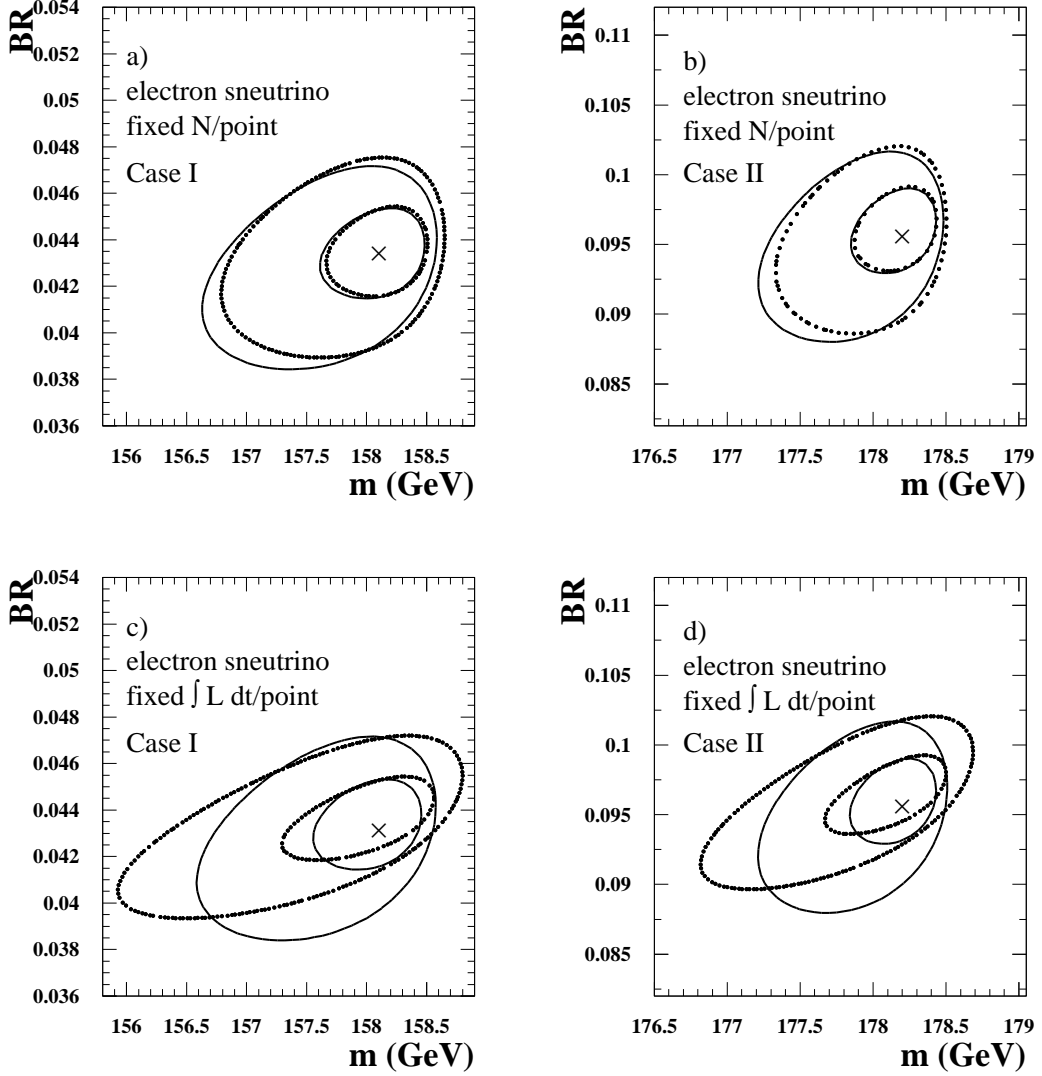


FIG. 14. 90% CL ($\Delta\chi^2 = 4.6$) contours in the $m(\tilde{\nu}_e) - BR$ plane, with $N = 3$ and a minimum of six signal events for each energy point after reconstruction efficiency, beamstrahlung and ISR for Case I (first column) and Case II (second column). The solid (dotted) contours correspond to $\Delta = 1$ GeV (30 GeV). The inner (outer) ellipses correspond to a total integrated luminosity of 500 fb^{-1} (120 fb^{-1}) of which 100 fb^{-1} (20 fb^{-1}) is at $\sqrt{s} = 500$ GeV. In the first row, the luminosity is distributed so that there are an equal number of events at each of the three low energy points, while in the second row the luminosity is equally shared between the three points. The cross shows the best fit for the $\Delta = 1$ GeV scan with 500 fb^{-1} .

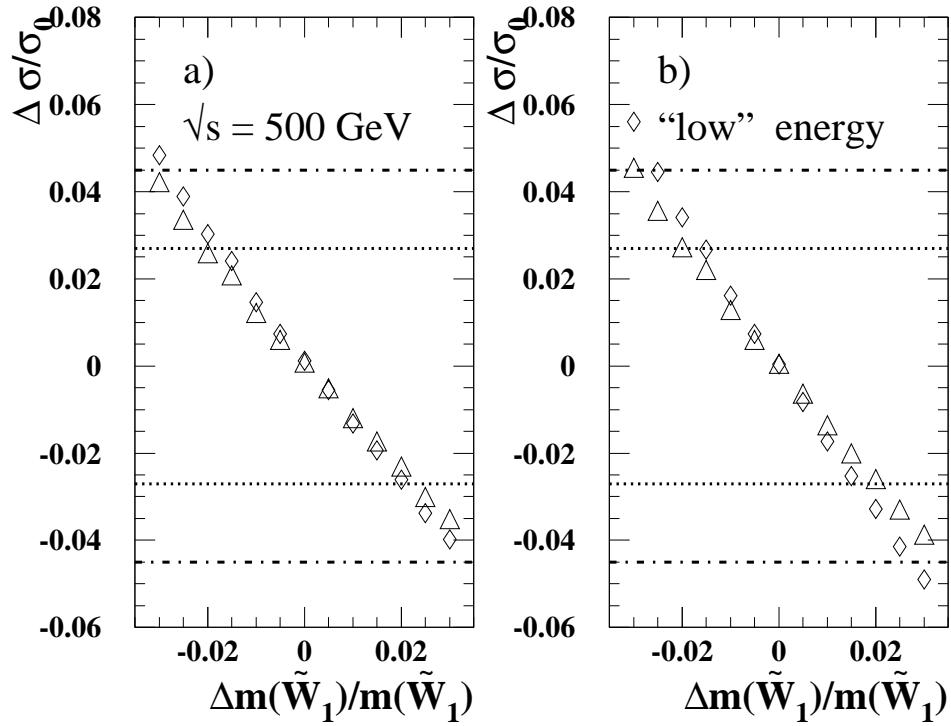


FIG. 15. The maximum fractional change in $\sigma(e^+e^- \rightarrow \tilde{\nu}_e\tilde{\nu}_e)$ from variation of the \tilde{W}_1 and \tilde{W}_2 masses within their expected uncertainty as a function of the precision of $m(\tilde{W}_1)$ for a) $\sqrt{s} = 500$ GeV, and b) $\sqrt{s} = 2m(\tilde{\nu}_e) + 2$ GeV. We assume that $\Delta m(\tilde{W}_2)/m(\tilde{W}_2) = 5\Delta m(\tilde{W}_1)/m(\tilde{W}_1)$. The diamonds show the results for Case I whereas the triangles show the same for Case II.